Economic Geology, v. 101, pp. 1359–1376

The Genesis of the Hope Downs Iron Ore Deposit, Hamersley Province, Western Australia

DESMOND F. LASCELLES†

Centre for Exploration Targeting, School of Earth and Geographical Sciences, University of Western Australia, 35 Stirling Highway, Crawley, W.A. 6009, Australia

Abstract

The banded iron formation (BIF)-hosted Hope Downs high-grade hematite ore deposits are situated within the Marra Mamba Iron Formation with subsidiary deposits in the Brockman Iron Formation of the Archean to Proterozoic Hamersley Group of Western Australia. The main orebody extends to 260 m below the surface and is unusually rich in martite (pseudomorphous hematite after magnetite) and poor in limonite and goethite compared to other ore deposits of the Marra Mamba Iron Formation. The high-grade hematite ore is mainly within the Newman Member but also occurs in parts of the Nammuldi Member together with low-grade limonitic ore that becomes high grade after calcining. Karst erosion of the overlying Wittenoom Formation has produced steep-sided buried valleys adjacent to the in situ orebodies that contain thick deposits (<160 m) of goethitic and sideritic sediments, including remnants of Robe Pisolite Formation, bedded siderite, hematite gravels, red ochreous detrital material, and enriched scree deposits that are additional sources of ore.

The ore consists of low phosphorous martite-limonite-goethite derived from chert-free BIF by supergene weathering. No evidence of the complete carbonate replacement of chert has been found at Hope Downs nor were any traces of preexisting chert bands seen in the ore, despite the abundance of chert bands in BIF elsewhere. A variety of textures and composition shown by cherty BIF adjacent to the orebodies is described from which the origin of the chert-free BIF is inferred, including sedimentary structures consistent with density-current deposition.

A model is presented for the origin of the host iron formation and the ore deposits, in which density currents transported reworked iron silicates and hydroxides in colloidal suspension onto an unstable sea floor. The amorphous silica produced during diagenesis of Al-poor iron silicates formed the characteristic chert bands of BIF but some of the hydrous amorphous silica was lost prior to lithification to form chert-free BIF. Weathering of the chert-free BIF produced the high-grade hematite ore that is exposed today.

Introduction

HOPE DOWNS is located approximately 75 km northwest of Newman (Fig. 1) in Western Australia. The main hematite ore deposits at Hope Downs (Fig. 2) are in the upper part of the Marra Mamba Iron Formation of the Hamersley Group (Fig. 3) with additional ore in enriched clastic deposits and in the nearby Brockman Iron Formation.

The Western Australia Geological Survey mapped the area at a regional scale in the 1960s, and company geologists carried out some reconnaissance mapping of the deposits together with limited test drilling during the 1970s and 1980s. Extensive reverse circulation percussion and diamond drilling, followed by detailed surface mapping and underground development, commenced in 1988.

The Marra Mamba Iron Formation and its hosted ore deposits at Hope Downs have been described previously by Paquay and Ness (1998) and (Lascelles, 2000, 2002). This paper is the second of two papers on the Mount Gibson and Hope Downs deposits, originally described in the conference proceedings of Iron Ore 2002 (Lascelles, 2002). In this paper, the sedimentologic and petrographic evidence for the origin of the ore deposits and the chert-free BIF from which they were formed are examined more closely. Samples were collected during surface (1:1000 scale) and underground mapping (1 adit and 10 winzes, 1:100 scale), reverse circulation percussion drilling (1,396 holes for a total of 113,183 m), and diamond coring (156 holes for a total of 20,989 m; R.D. Paquay, pers. commun., November 2004).

† E-mail address: dlascell@segs.uwa.edu.au

Regional geology

Hope Downs is centrally located near the eastern end of the Hamersley province (Fig. 1), which is an elliptical area of Archean to Paleoproterozoic metasedimentary and volcanic rocks, comprising the Mount Bruce Supergroup (Fig. 3) and overlying the granitoids and greenstone belts of the Pilbara craton (Trendall and Blockley, 1970; Trendall, 1979). The Mount Bruce Supergroup is divided into three Groups. The basal Fortescue Group, deposited between 2.8 to 2.6 Ga (Richards and Blockley, 1984), consists of thick volcanogenic and minor clastic and chemical sedimentary rock units unconformably deposited on the basement granitoids and greenstones. The Fortescue Group is conformably overlain by the Hamersley Group of predominantly chemical sedimentary rocks, deposited between 2.6 to 2.4 Ga (Compston et al., 1981; Trendall et al., 2004), with lesser ash-fall deposits (La Berge, 1966, Pickard et al., 2001, 2004) and intrusions. The Turee Creek Group conformably overlies the Hamersley Group and represents a return to shallow-water terrigenous clastic and chemical sedimentation, prior to uplift, erosion, and the subsequent deposition of the Wyloo Group. The Mount Bruce Supergroup is unconformably overlain by the Wyloo Group at its south and west margins but no evidence remains of the Wyloo Group in the northern and eastern parts of the Hamersley province.

The Marra Mamba Iron Formation defines the base of the Hamersley Group and conformably overlies the Jeerinah Formation of the Fortescue Group (Davy, 1975; Davy and Hickman, 1988). The overall stratigraphy of the Marra Mamba

0361-0128/06/3624/1359-18

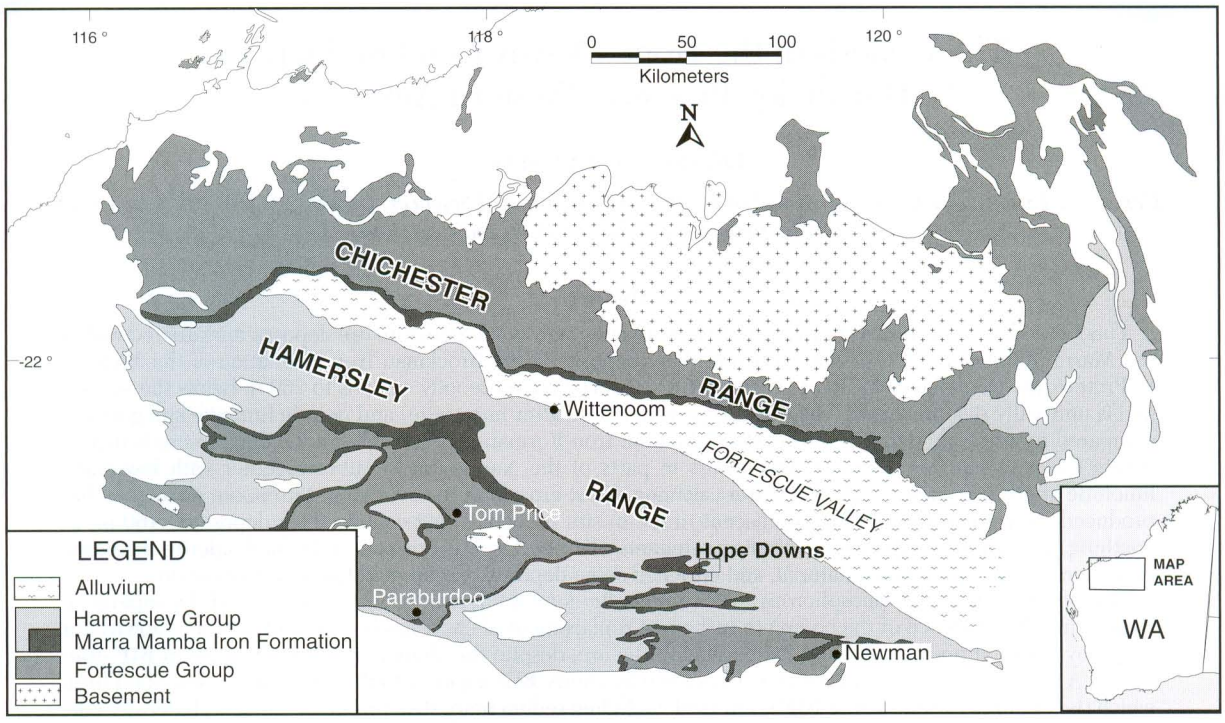

FIG. 1. Simplified regional geology of the Hamersley province, W.A.

Iron Formation (Trendall and Blockley, 1970; Blockley et al., 1993) is uniform throughout the Hamersley province, at least to the macroband level (i.e., banded iron formation and shale bands), with only minor variations in thickness. The division of the formation into numbered macrobands has been formalized for the upper two members, but due to general lack of interest in the Nammuldi Member by mining companies and the absence of complete measured sections, the subdivision of the Nammuldi Member is informal (Blockley et al., 1993).

The overlying Wittenoom Formation is typically deeply eroded and is poorly exposed in valleys between the iron formations that are typically filled with thick accumulations of Phanerozoic (Tertiary to Recent) detrital deposits. Mature karst topography, largely buried by valley fill sediments, was discovered during drilling with subvertical to overhanging valley walls, isolated pinnacles, and arches left by collapsed cave systems. Ferricrete remnants of various origins locally form low mesas and commonly occur around the sides of the valleys or may be buried by recent alluvial sediments.

Two major folding events, the ca. 2140 Ma Ophthalmian orogeny, the minor Panhandle folding event at ca 2008 Ma, and the ca. 1770 Ma Capricorn event and (Müller et al., 2005) have affected the Hamersley province with strong folding, faulting, and thrusting along the southern, western, and eastern margins, diminishing to the north. Folding styles are highly variable, depending on the competency and thickness of the folded strata and the age of the folding. Upright concentric folding appears to be related to the Ophthalmian major dome and basin structure of the Hamersley province (D_{2oph} of Müller et al., 2005). Simple broad-scale folding with a visible cleavage or schistosity is characteristic of the 300-m-thick Joffre Member BIF although small-scale accommodation folding may be abundant locally. Cleavage is very rare in other iron formations. The Dales Gorge Member and the Marra Mamba Iron Formation typically display concentric and less commonly chevron-style folding, and the more thinly bedded and less competent strata, such as the Whaleback Shale, Mount McRae Shale, and Mount Sylvia Formation, show much tighter, almost convoluted folding. Lack of exposure prevents drawing generalizations about the style of folding in the Wittenoom Formation, but broad open folding is inferred from the few outcrops. Superimposed on this structure are a number of typically chevron-style minor folds that appear to be related to the Capricorn event (D_{2cap} of Müller et al., 2005).

Burial metamorphism to prehnite-pumpellyite greenschist facies has affected the central part of the province, with increasing metamorphism in the eastern and western margins, rising to actinolite greenschist facies along the southern margin (Smith et al., 1982). All minerals in Hamersley Group BIF were recrystallized during diagenesis and metamorphism, and there is no trace of original granules or terrigenous clastic material.

Geology of the Hope Downs Area

Geomorphology

The Marra Mamba Iron Formation typically forms gently rounded low hills; however, cliffs up to 30 m high commonly form at the base of the Nammuldi Member and in narrow gorges. Nearly flat-lying cherty BIF of the Nammuldi Member, with two small inliers of Jeerinah Formation, forms the core of the the Weeli Wolli anticline, with the upper Marra Mamba Iron Formation exposed in a central subsidiary syncline and on the flanks of the anticline (Figs. 2, 4). Deep

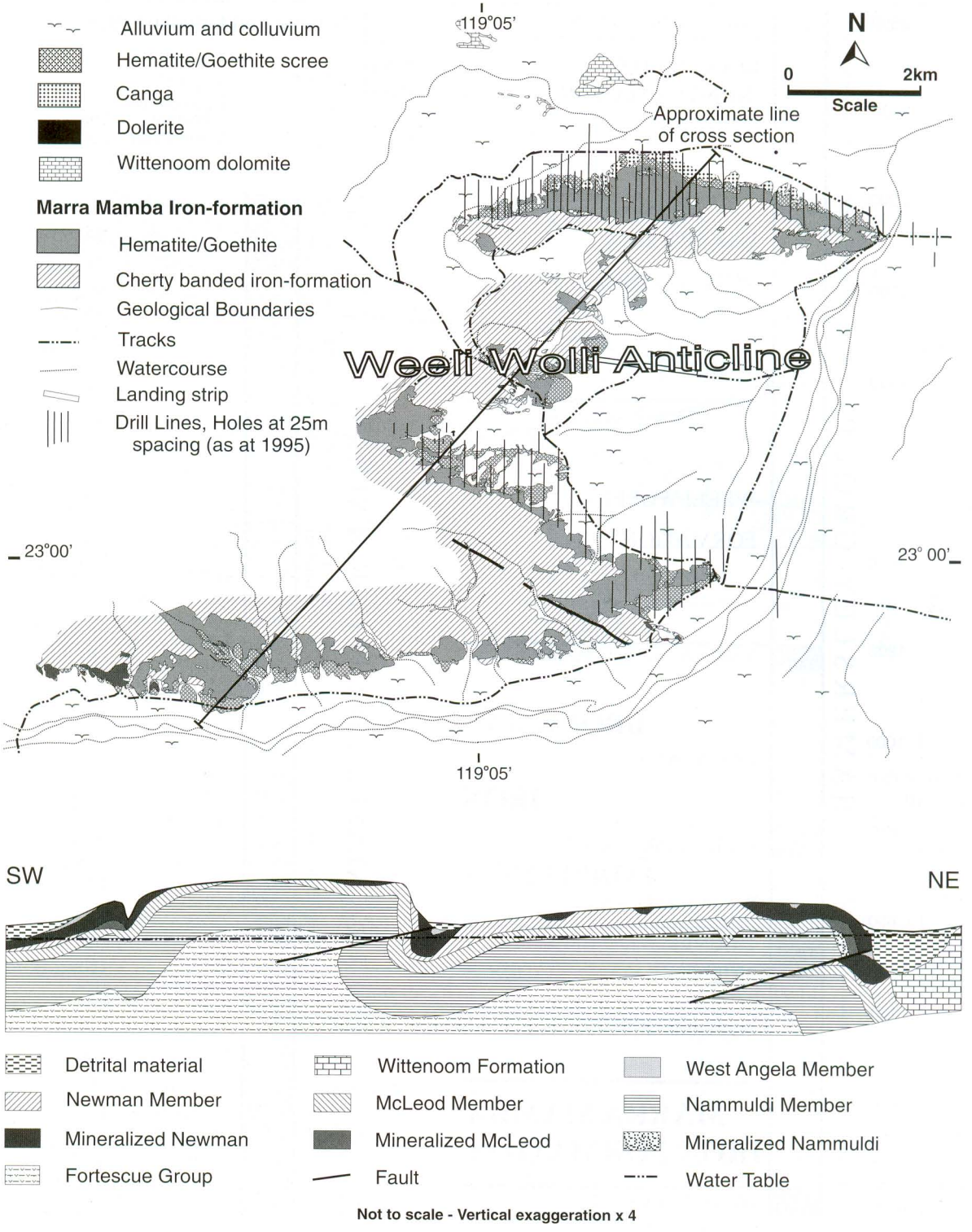

FIG. 2. Geologic map and cross section of the Hope Downs iron ore deposit from Lascelles (2002).

buried valleys incised into the overlying Wittenoom Formation lie to the north and south of the anticline and subsidiary valleys have eroded narrow ravines and box canyons in the iron formation.

Numerous caves occur within the superficial iron formation mainly due to the elutriation of fine particles by tunnel erosion along joints and bedding planes, with enlargement by roof collapse. Many side valleys, particularly in subhorizontal strata, have a characteristic box canyon profile of comparatively flat floors with steep cliffs at the side and head of the valley, probably due to major tunnel erosion followed by roof collapse.

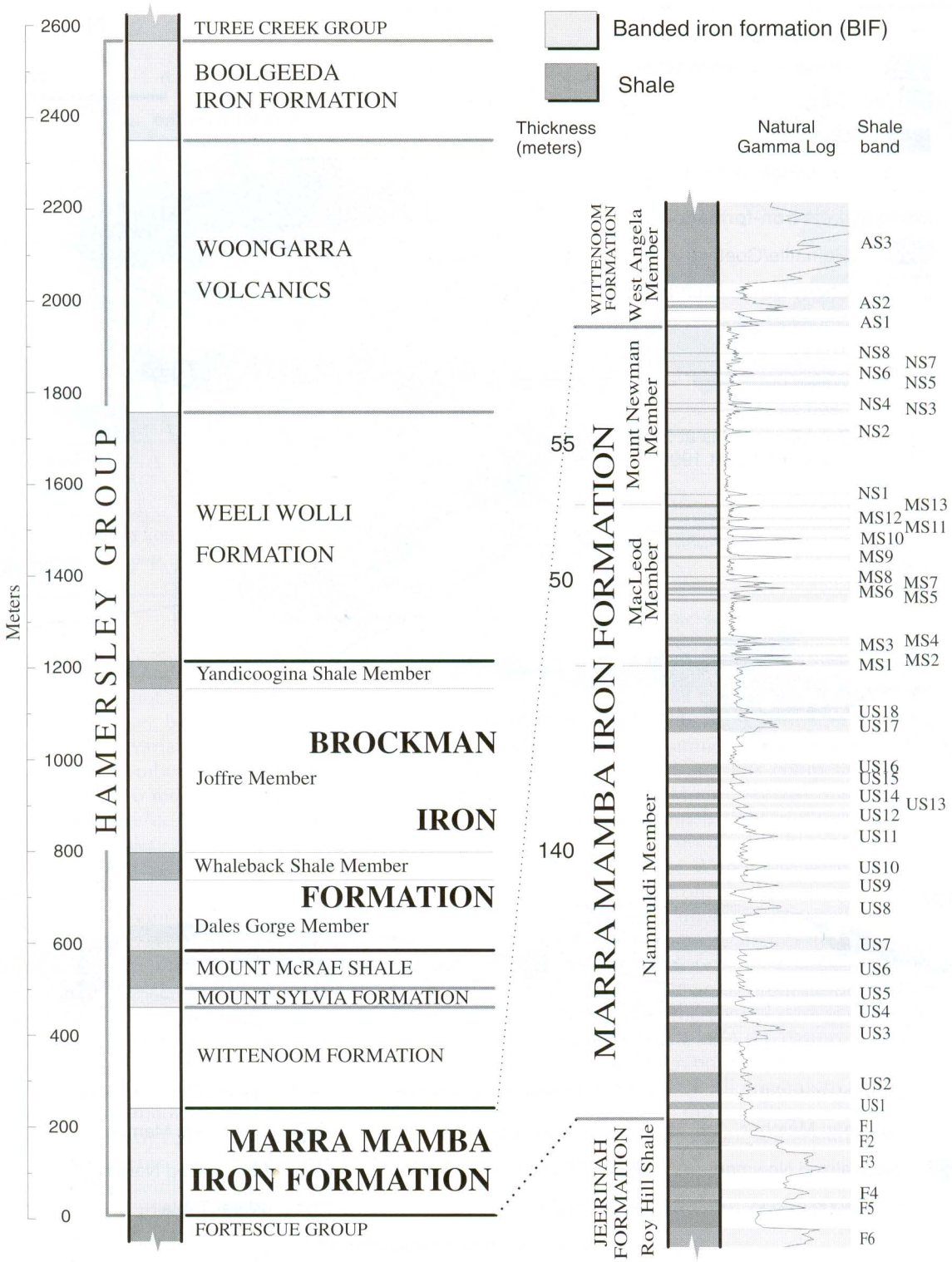

FIG. 3. Stratigraphy of the Marra Mamba Iron Formation (drawn by F. Talen, Rio Tinto Iron Ore) from Lascelles (2000).

The regolith shows signs of prolonged development with weathering of the saprolite (Jackson, 1997) to depths locally in excess of 300 m below the surface. The water table is essentially flat, ranging from 3 to 10 m below the level of the riverbeds and falls away at approximately 1 m/km perpendicular to the river channels (D. Lascelles, unpub. report for Pennant Resources Ltd., 1990), indicating recharge from the rivers during flood periods. Current rainfall rarely penetrates more than 3 m below the surface even in the wettest seasons, except down open joints or cavities, and the solum (Jackson,

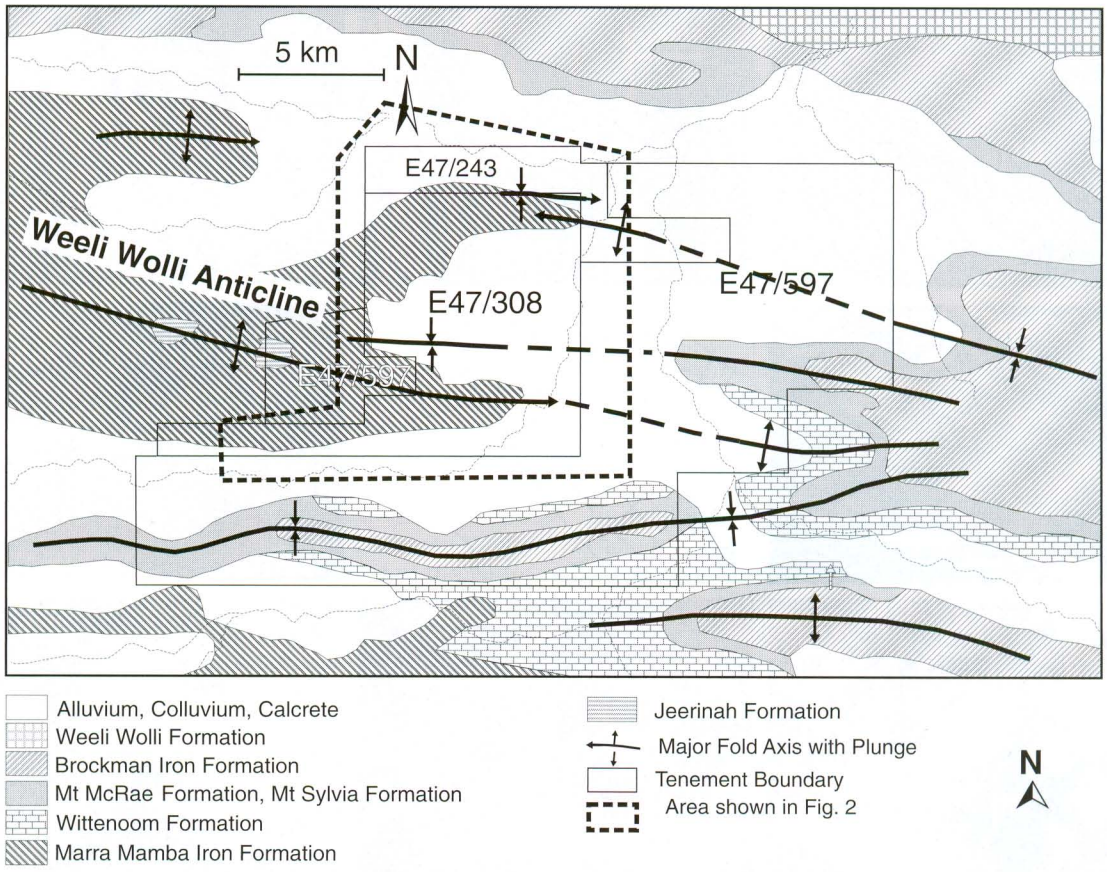

FIG. 4. Major structures within the Hope Downs area (modified after Paquay and Ness, 1998).

1997) is typically in an arrested stage of development with saprolite above the current water table commonly showing only minor alteration by soil processes.

Stratigraphy and lithologic units

Bedrock units of the Mount Bruce Supergroup ranging from the Jeerinah Formation to the upper Brockman Iron Formation (MacLeod, 1966; Trendall and Blockley, 1970) are exposed at Hope Downs (Fig. 3). Tertiary to Recent fluvial detrital rocks deposited in deep valleys eroded into the Wittenoom Formation unconformably overly the Mount Bruce Supergroup.

Although the Marra Mamba Iron Formation shows great variability in mineralogy, thickness, and texture of individual bands, some generalizations can be made that are characteristic of the Formation and allow rapid field identification. The Formation is typified by coarser banding than most of the other BIF of the Hamersley Group, with mesobands commonly between 2 to 10 cm thick and rarely ranging up to 30 cm thick. The magnetite mesobands and iron silicate-carbonate mesobands typically display fine microbanding under the microscope (Fig. 5A, B) and traces of microbanding are visible in chert layers (Fig. 5C) in the form of fine iron oxide, amorphous carbon, and silicate laminae. The trace minerals typically form faint laminations parallel to the overall banding and can be traced into laterally adjacent iron silicate bands. Fresh broken or polished surfaces of the chert bands are colored very dark green or deep blue by these trace minerals.

The proportion of silicates and carbonates in chert bands typically increases near the contacts with other mesobands; mixed bands of silicate and carbonate typically occur between chert and magnetite mesobands. The exposures range from flat tabular sheets to complex rippled sheets (Fig. 5D, E), anastomozing lenses, elongated rods, and rounded to elliptical pods. Imbricated lenticular pods with anastomozing magnetite bands are associated with particular chert bands and may be traced along outcrops for hundreds of meters but rarely may occur localized in bands crosscutting the layering at a sharp angle (Fig. 5F). Many chert pods show external or internal shrinkage cracks filled with clear crystalline quartz. Weathered chert bands are typically degraded to a friable silty consistency by dissolution of amorphous silica around grain boundaries (Yariv and Cross, 1979) but they show no evidence of dissolution of the residual quartz grains. Surface exposures of friable weathered cherty BIF are typically cemented by secondary silica, and similarly the migration and deposition of secondary silica typically produces a small increase in the silica content of chert-free ore (<10 wt %) near the contact with cherty BIF (~45 m, Fig. 6).

A stratigraphic reference hole (HDD9043, see graphic log in Fig. 6) was drilled through gently dipping strata on the southern flank of the Weeli Wolli anticline and passed through the ore-grade West Angelas and upper Mount Newman Members into the unweathered MacLeod and Nammuldi Members BIF. Unfortunately, the Mount Newman Member, which is the most studied and productive part of the

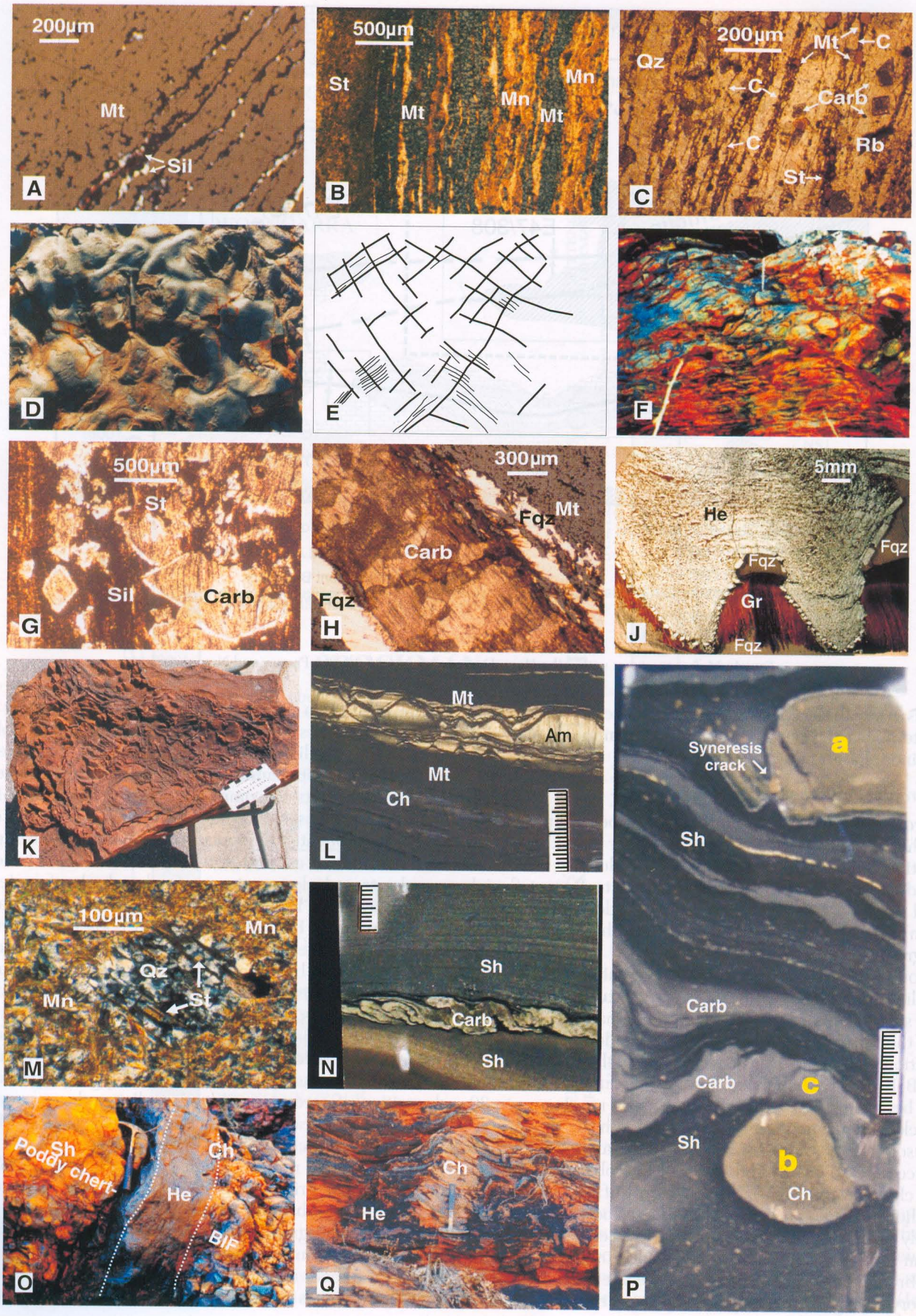
200µm
Mt
Sil
A
500µm
St
Mt
Mn
Mn
Mt
B
200µm
Qz
Mt
C
C
Carb
C
Rb
St
C
D
E
F
500µm
St
Sil
Carb
G
300µm
Fqz
Mt
Carb
Fqz
H
5mm
He
Fqz
Fqz
Gr
Fqz
J
K
Mt
Am
Mt
Ch
L
100µm
Mn
Qz
Mn
St
M
Sh
Carb
Sh
N
Syneresis crack
a
Sh
Carb
Carb
c
Sh
b
Ch
P
Sh
Poddy chert
Ch
He
BIF
O
Ch
He
Q

Marra Mamba Iron Formation, was strongly weathered in all drill cores and highly deformed except in the stratigraphic hole. An approximate true stratigraphic thickness of 70 m, including 10 m of chert-free ore (35–45 m), was obtained from the stratigraphic hole and compares to an average thickness of 54 m for the Mount Newman Member high-grade ore at Hope Downs. BIF macrobands are typically coarse, essentially monomineralic bands of magnetite and chert (avg 5 cm thick) separated by iron silicate-carbonate mesobands. Leaching and oxidation of the iron carbonate and silicates leave a residue of limonite that imparts a yellowish coloration to the Marra Mamba Iron Formation outcrops.

Outcroppings of the cherty upper Mount Newman Member are very rare at Hope Downs with only a small exposure of the top few meters adjacent to the main access road south of the airstrip turnoff. The exposure contains very large football sized ovoid chert pods with coarsely crystalline quartz-filled internal shrinkage cracks in anastomosing magnetite mesobands. All other exposures of the upper Newman Member are chert free. Cherty BIF of the lower part of the Newman Member (below NS3, Fig. 3) forms an almost continuous outcrop around the flanks of the Weeli Wolli anticline, except where interrupted by high-grade ore of the major ore deposits. Delamination of oxide mesobands with the insertion of abundant cross-fiber quartz bands and lenses is very common in NB1 (between NS1 and NS2, Fig. 3) and also in the oxide mesobands of the MacLeod Member but is not seen in ore. Strong deformation, metamorphism, and deep weathering typically obscure sedimentary structures and textures within the Mount Newman Member at Hope Downs, and the ubiquitous iron staining and differential erosion of outcrops, particularly at BIF-shale contacts, make detailed observations difficult. Apart from the laminations and banding, truncated ripple bedding at BIF-shale contacts and sole markings on bedding planes are the only sedimentary structures that can be confidently identified in the Mount Newman Member.

Silicate-chert-carbonate bands: Silicate bands, with abundant carbonate and chert ("SCC bands" of Morris, 1991) divide the Marra Mamba Iron Formation into a series of BIF macrobands (Figs. 3, 6). Although commonly described and labeled as shale or "S" bands nearly all silicate-chert-carbonate bands fall into the carbonate facies of BIF (sensu stricto James, 1954) and consist mainly of interlayered siderite-ankerite and chert mesobands with minor stilpnomelane, minor carbon-rich black shale bands, and very rare magnetite laminations or disseminated grains. Some chert-free sections include mesobands of minnesotaite. The siderite typically shows a texture of interlocking subhedral crystals and is rapidly oxidized to cryptocrystalline hematite or goethite on exposure. Solid drill core (NQ) was oxidized to a depth of 3 mm in 10 mo and completely oxidized in 3 yr. Unfortunately no samples were preserved from atmospheric oxidation and no specimens currently exist of the original unweathered siderite. Stilpnomelane forms thick mesobands, laminae, and disseminations in the silicate-chert-carbonate bands and is a minor accessory mineral throughout the BIF macrobands. Some of the stilpnomelane mesobands are strongly carbonaceous and pyritic (black shale), and thin carbonaceous stilpnomelane bands are common as partings in the BIF macrobands.

In outcrop and in weathered ore zones, the silicate-chert-carbonate bands are reduced to bands of multicolored kaolinite (with the addition of friable chert bands when originally present), ranging from white to various shades of red, brown, and gray (cf. Webb et al., 2003) after leaching of the carbonate. Iron is typically concentrated in the form of goethite nodules with a characteristic luster and olive-brown color, which can delineate shale subcrops after the kaolinite has also been removed by surface erosion.

BIF macrobands: The BIF macrobands in the MacLeod and Nammuldi Members at Hope Downs typically consist of alternating laminar to strongly podded chert mesobands, iron carbonate-iron silicate mesobands, and finely laminated or disseminated magnetite in iron silicate mesobands. These bands are readily hydrated to goethite during weathering, resulting in lower iron ore grades. The MacLeod Member is distinguished from the Nammuldi Member by the greater frequency of silicate-chert-carbonate bands and carbonates causing outcrops to be typically more strongly weathered and eroded. Coarse mesobands of magnetite occur rarely over narrow intervals at the top of some major BIF macrobands and predominate over a ~20-m-thick zone, ~30 m below the Nammuldi-MacLeod contact (~205–225 m: Fig. 6).

The Newman Member also contains abundant massive magnetite mesobands that are less susceptible to hydration

FIG. 5. A. Laminations in magnetite mesoband (plane-polarized transmitted and reflected light). B. Finely laminated magnetite and silicate BIF (plane-polarized transmitted and reflected light) from Lascelles (2002). C. Trace laminations of fine-grained stilpnomelane, dusty magnetite, and carbon in chert (plane-polarized transmitted and reflected light) from Lascelles, (2002). D. Upper surface of chert layer, showing pinch and swell and microfractures in chert. E. Pattern of intersecting wave crests (thick lines) and microfractures (thin lines) in (D). F. Imbricated chert pods in otherwise planar cherty BIF. Length of pencil is 15 cm. G. Coarse subhedral to euhedral carbonate replacing minnesotaite in silicate mesoband (plain transmitted light). H. Fine laminated silicate band completely replaced by carbonate (plane-polarized transmitted and reflected light). J. Pseudomorphous goethite after asbestiform riebeckite (griqualandite), showing the structure of hematite at the upper contact. K. Underside of magnetite mesoband in contact with asbestos seam (asbestiform riebeckite removed by weathering). L. Asbestiform amosite seam (cut surface of split core, scale divisions are1 mm). M. Pseudomorphous microcrystalline quartz after rhomboid carbonate with flakes of recrystallized stilpnomelane oriented along crystallographic planes (crossed nicols) from Lascelles (2002). N. Convoluted bedding caused by current drag on newly deposited fine-grained carbonate (scale divisions 1 mm). O. Debris dike in Nammuldi Member BIF, Wonmunna Gorge (dotted outline). P. Inverted rip-up clast in shale (a) with hardened skin and rectangular cross section from syneresis cracks. Globular chert clast (b) showing hardened skin, deformed by current drag that also convoluted the overlying carbonate band (c). Q. Clumping of boudinaged chert pods into vertical stacks during slumping. Am = amosite; C = carbon; Carb = carbonate; Ch = chert; Fqz = fibrous quartz; Gr = griqualandite; He = hematite; Mn = minnesotaite; Mt = magnetite; Qz = quartz; Rb = riebeckite; Sh = shale; Sil = undifferentiated iron silicates; St = stilpnomelane.

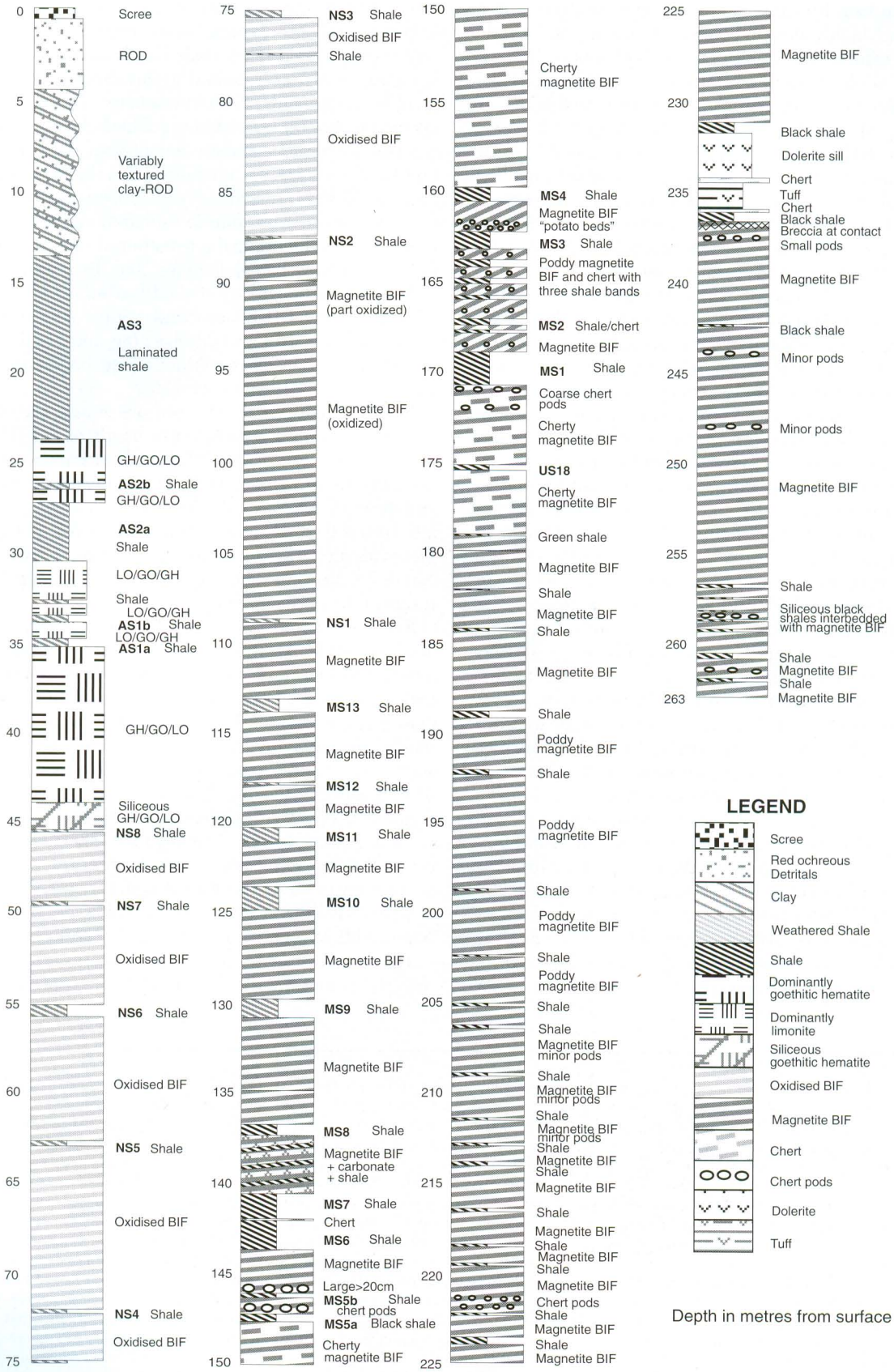

FIG. 6. Graphic log of HDD9043. BIF = 3D cherty banded iron-formation, GH = 3D goethitic hematite, GO = 3D goethite, LO = 3D limonite, ROD = 3D red ochre detritals.

and are preserved as hematite (high-grade ore). The chert in these units is highly variable in texture both laterally and vertically, ranging from evenly banded through podded to contorted.

Iron silicate mesobands: Iron silicate minerals are abundant in the unweathered Marra Mamba Iron Formation and typically form mesobands with carbonate minerals between the chert and the magnetite bands. The Marra Mamba Iron Formation in Hope Downs contains abundant minnesotaite, stilpnomelane, and riebeckite but no grunerite, greenalite, or chlorite was observed (i.e., corresponding to the minnesotaite metamorphic zone of Miyano, 1987). Recrystallization of minnesotaite is common locally, producing a coarser grained decussate texture and comb structure in fractures, and stilpnomelane commonly shows a coarse bladed texture along the fringes of stilpnomelane-rich bands. Carbonate metasomatism is abundant (Fig. 5G, H) and fine millimeter-scale quartz and quartz-carbonate veins are common.

Seams of cross-fiber asbestiform riebeckite (crocidolite) rarely exceeding 5 cm in thickness and fibrous quartz are abundant at certain horizons within the Marra Mamba Iron Formation. The asbestiform riebeckite seams occur on both limbs and hinges of folds (i.e., in both extensional and compressional areas) and are folded together with the adjacent BIF layers. The seams typically occur between magnetite mesobands (Beukes, 1980) but very rarely occur within nonasbestiform riebeckite mesobands or may be underlain by chert. They show a unique morphology against the stratigraphically upper magnetite contact with abundant dependent cones and ridges of magnetite that are rarely seen against the lower contact (Fig. 5J, K). Rare seams of cross-fiber asbestiform amosite (Fig. 5L) may occur adjacent to crocidolite seams but are more commonly within shale bands widely separated from riebeckite occurrences. Goethite is pseudomorphous after crocidolite seams in the ore that are comparatively rare (griqualandite, Fig. 5J). Nonasbestiform mesobands of decussate riebeckite up to 20 cm thick occur locally and have been observed to pass laterally into chert bands (Trendall and Blockley, 1970) but more commonly pinch out between magnetite mesobands, as do the crocidolite seams.

Although the massive carbonate replacement of chert seen in parts of the Mount Gibson Iron Formation (Lascelles, 2006), Koolyanobbing, and Mount Tom Price (Taylor et al., 2001) is not seen at Hope Downs, there is extensive replacement of silicates by carbonate (Fig. 5G, H) and considerable replacement and interaction between quartz and carbonates is ubiquitous (Fig. 5M).

Lithologic variations and primary structures: Lateral variations in lithology within the Marra Mamba Iron Formation are evident on a large scale by the absence of chert bands within the ore zones and on smaller scales by marked variation in chert podding, crocidolite bands, carbonate content, and silicate mineralogy. Some of these variations may be due to tectonic deformation and metamorphism, but others are primary or have a diagenetic origin.

Numerous sedimentary structures characteristic of current deposition were visible in the MacLeod and Nammuldi Members. Small-scale current bedding with frequent changes of dip and fine ripple bedding is common in finely laminated strata but is typically confused or obscured by podding in thickly mesobanded BIF. Layers of fine-grained carbonate are interpreted as pelagic calcareous ooze. The typical convolutions are interpreted to be caused by current drag on the fine sediments (Fig. 5N). Small-scale graded bedding is commonly present but, due to the high-density contrast between the sedimentary particles, grading is by density rather than particle size. Flame structures and disks of chert are common features, suggesting a highly fluid saturated and mobile iron hydroxide layer during early diagenesis. Rare microscale dewatering structures were observed and even more rare debris dikes (Fig. 5O) and magnetite veins, consisting predominantly of iron oxide clasts with little or no interstitial chert or chert clasts.

Locally silicified horizons display a flat to eroded upper surface and irregular penetrative lower surfaces in both shale and BIF (Krapez et al., 2003). The silicified surface commonly shows numerous syneresis cracks with corresponding rectangular rip-up clasts in the overlying shale (Fig. 5P a).

Globular to elliptical chert pods (Fig. 5P b) are common throughout the silicate-chert-carbonate macrobands and basal portions of BIF macrobands in the Marra Mamba Iron Formation and range in size from a few millimeters to >30 cm in diameter. Concentric internal zoning of chert pods showing differing rates of lithification from the surface of the nodule is typical. The larger pods commonly display stellate internal shrinkage cracks, which are typically filled with coarsely crystallized quartz, and rarely various species of $(Fe,Mg,Ca)CO_3$ with minor hematite, around an ellipsoidal chert center, indicating the development of a hardened skin prior to syneresis. When abundant, they accumulate to form such distinctive layers as the "potato bed" in the MacLeod Member and particularly large examples form the distinctive horizon near the top of the Mount Newman Member at Hope Downs.

Intraformational folding, due to soft-sediment creep and slumping, is common in the BIF members, with styles ranging from upright concentric to overturned asymmetric and chaotic folds, and appears to equate with the D_{1c} folding of Tyler and Thorne (1990). Small- to medium-scale segregations of chert and iron oxides form during slumping of semiconsolidated sediment with clumping of boudinaged soft chert bands into vertical stacks (Fig. 5Q). A typical slump shows evenly banded BIF gradually transformed into podded and deformed chert bands culminating in complex folds passing abruptly back into evenly banded BIF, with little variation in the overall thickness of the BIF macroband. The slump features typically involve only part of a macroband and rarely more than one macroband and are typically bounded by undeformed strata. No stratigraphic breaks or erosion scours were observed associated with the intraformational folds.

Structure

The Hope Downs deposit lies on the eastern end of the east-west–trending Weeli Wolli anticline, which plunges to the east and the west, forming an elongated dome with minor plunge reversals along the axis and numerous subsidiary folds (Fig. 4). The central part of the Weeli Wolli anticline is characterized by flat-lying to gently dipping strata that very abruptly turn into steeply dipping synclines plunging to the east at Hope Downs (Fig. 2). Major folds have south-dipping

axial planes with a general east-west strike with en echelon minor folds striking west-northwest-east–southeast to west-southwest–east-northeast. These structures extend across the valley of the Weeli Wolli creek into the synclinal outcrops of the Brockman Formation on the eastern side of the tenements (Fig. 4).

Intense deformation of cherty BIF with crushed and contorted chert and magnetite mesobands and abundant fibrous quartz and riebeckite (Fig. 7A, B) is associated with low-angle thrusts dipping to the south-southeast on the northern limbs of the main central syncline and the northern margin of the Weeli Wolli anticline (Fig. 2) but, apart from the juxtaposition of Marra Mamba Iron Formation on the West Angela Member and the Nammuldi Member on the Mount Newman Member, the thrust planes are rarely distinguishable in the ore or in outcrops due to the pervasive brecciation. Minor stress relief faults, in which displacement rarely exceeds a few meters that are typical of dome and basin structures, are seen in underground exposures of the ore but are rarely discernable in outcrop except where the displacement of shale bands can be seen. Millimeter-scale microfaults restricted to the chert bands are typically abundant, illustrating the brittle character of the chert during deformation (Fig. 5D, E). However, the chert is both plastically deformed and brecciated in the intensely deformed thrust zones (Fig. 7A, B).

Deformation is more complex in ore due to pervasive localized brecciation and crumpling, caused partly by volume changes due to loss of chert bands and partly as a result of differential competence between the chert-free and cherty BIF. Folding styles vary according to the hardness and competency of the ore, ranging from cylindrical folds in finely laminated ore to chevron folds in more competent coarsely mesobanded material.

Hope Downs Iron Ore Deposits

The high-grade orebodies within the Marra Mamba Iron Formation consist of two major deposits and several minor orebodies scattered throughout the area. The Hope North deposit has proven reserves of 337 million metric tons (Mt) at 61.6 wt percent Fe, 2.9 wt percent SiO_2, 1.5 wt percent Al_2O_3, 0.06 wt percent P, and 7.1 wt percent LOI and extends for 7 km along the northern limb of the Weeli Wolli anticline (Paquay and Ness, 1998). The Hope South deposit, with proven reserves of 185 Mt at 61.6 wt percent Fe, 3.5 wt percent SiO_2, 1.8 wt percent Al_2O_3, 0.06 wt percent P, and 6.2 wt percent LOI (Paquay and Ness, 1998), lies on the southern flank of an easterly plunging syncline and continues around the southern limb of the Weeli Wolli anticline (Fig. 2). High-grade hematitic iron ore (>60 wt % Fe) occurs mainly within the Mount Newman Member and a small section of the Nammuldi Member (Fig. 3) as subhorizontal to shallow-dipping deposits in the plateau areas and south-facing slopes and complexly folded deposits flanking and partially underlying deep detritus-filled valleys in the north-facing limbs of the major folds. Hematite-goethite-limonite ore is continuous in places from the West Angelas Member of the Wittenoom Formation through the Mount Newman and MacLeod Members into the upper part of the Nammuldi Member of the Marra Mamba Iron Formation (Fig. 3).

The low-grade ore (50–60 wt % Fe) in the West Angelas and MacLeod Members consists mainly of limonite and goethite and typically contains high levels of alumina and silica (>10 wt %) from interbedded clay (i.e., weathered shale-carbonate-chert) bands; however, the low-grade part of the Nammuldi Member ore consists of limonite with minor goethite and gives calcined grades of up to 67 wt percent Fe and low alumina and silica (~2 wt %) contents. Ore grade is related to magnetite content and distribution in the original BIF, whereby abundant magnetite mesobands give rise to high-grade martite-goethite ore, but disseminated magnetite is readily hydrated to goethite giving lower Fe grades. The high-grade ore (60–62 wt % Fe) is up to 54 m thick on the plateau but reaches widths of over 200 m and depths of 260 m from the surface beneath the buried valleys. The high-grade ore in the plateau is fairly typical of the Marra Mamba Iron Formation and is characterized by abundant limonite and goethite, a thick hydrated zone and numerous cavities, but the deeper ore is unusually rich (>65 wt % Fe) with less than 15 percent limonite (by volume estimated from drill core) and very minor goethite.

FIG. 7. A. Intensely deformed Mount Newman Member (cut surface, slightly weathered core section, scale in mm) from Lascelles (2002). B. Mylonitic Newman Member (polished thin section, natural transmitted light). C. Well-developed martite trellis texture in partly weathered euhedral martite (plane-polarized reflected light). D. Euhedral magnetite overgrowths replaced by martite on primary laminae (plane-polarized reflected light). E. Magnetite overgrowths replaced by martite on multiple laminae fragments (plane-polarized reflected light). F. Goethite pseudomorphous after iron silicates (plane-polarized reflected and transmitted light); G. Goethite and limonite pseudomorphous after silicate and carbonate grains, respectively (plane-polarized reflected light). H. Limonite pseudomorphous after euhedral martite (plane-polarized reflected light). J. Bands of amorphous goethite probably after fine-grained carbonate with partially goethitized silicate minerals. Note unoxidized magnetite (plane-polarized transmitted and reflected light). K. Anhedral hematite and cryptocrystalline goethitic hematite derived from dispersed, redeposited, and dehydrated goethite and/or limonite (plane-polarized reflected light). L. Weathered BIF with unaltered euhedral pyrite, partially oxidized magnetite, and silicates and carbonates completely replaced by goethite (plane-polarized transmitted and reflected light). M. Brecciated magnetite mesoband with fibrous quartz pressure shadows (crossed nicols). N. Delaminated magnetite mesoband with fibrous quartz pressure shadows (crossed nicols). O. Zoned euhedral carbonate grains in chert (crossed nicols). P. Granules of siderite and dolomite in subhedral to skeletal carbonate grains (plane-polarized light). Q. Prismatic riebeckite grains in BIF (plane-polarized transmitted and reflected light). R. Sketch illustrating typical vertical distribution of pyrite in BIF (black = pyrite; dark gray = magnetite; light gray = iron silicate and carbonate; white = chert). S. Anhedral pyrite overgrowths on euhedral pyrite grain (plane-polarized reflected light). Carb = carbonate; Ch = chert; Fqz = fibrous quartz; Go = goethite; Go/He = cryptocrystalline goethitic hematite; GoSil = goethite pseudomorphous after iron silicates; 3Go = tertiary goethite; Lm = limonite; He = hematite; Mn = minnesotaite; Mr = martite; Mt = magnetite; Py = pyrite; Qz = quartz; Rb = riebeckite; Sil = undifferentiated iron silicates; Vo = void.

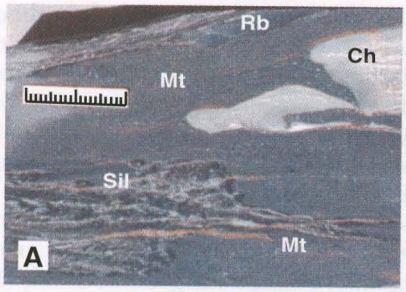
Rb
Ch
Mt
Sil
Mt
A

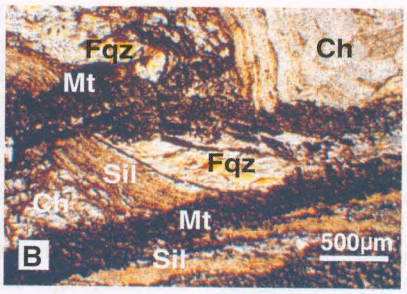
Fqz
Ch
Mt
Sil
Fqz
Ch
Mt
Sil
500µm
B

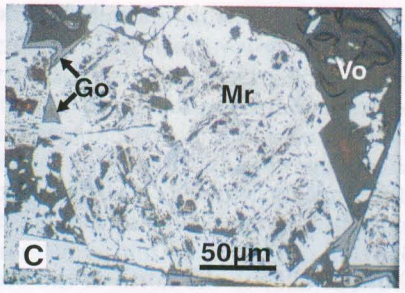
Go
Mr
Vo
50µm
C

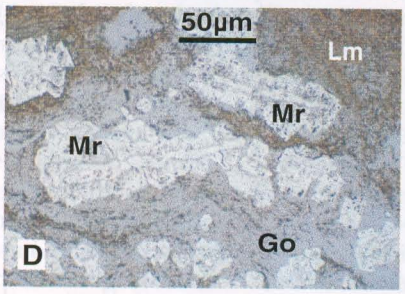
50µm
Lm
Mr
Mr
Go
D

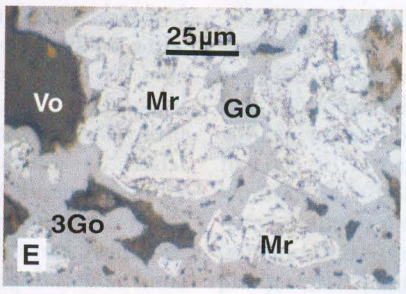
25µm
Vo
Mr
Go
3Go
Mr
E

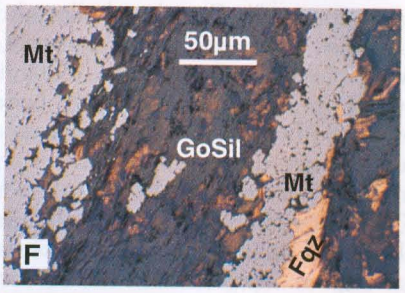
Mt
50µm
GoSil
Mt
Fqz
F

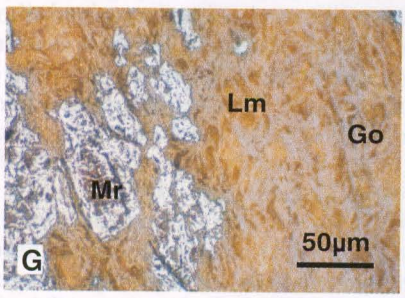
Lm
Go
Mr
50µm
G

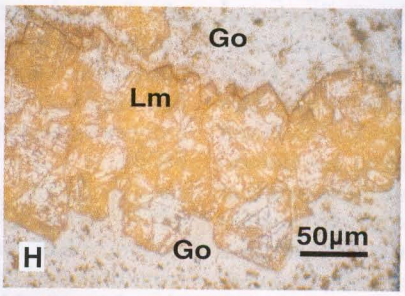
Go
Lm
Go
50µm
H

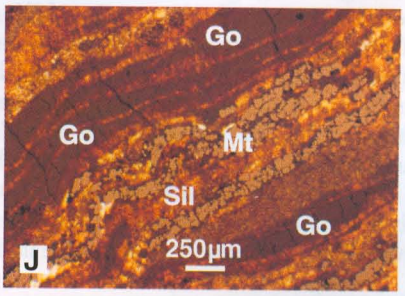
Go
Go
Mt
Sil
Go
250µm
J

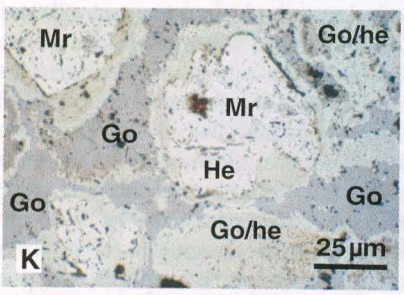
Mr
Go/he
Mr
Go
He
Go
Go
Go/he
25µm
K

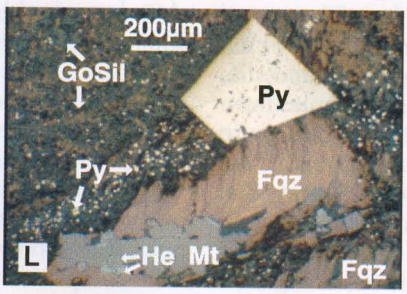
200µm
GoSil
Py
Py
Fqz
He
Mt
Fqz
L

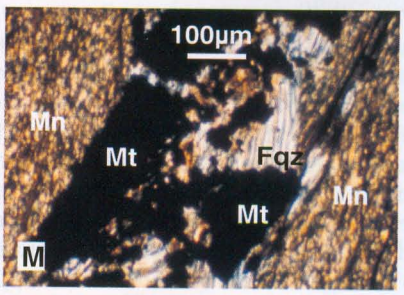
100µm
Mn
Mt
Fqz
Mt
Mn
M

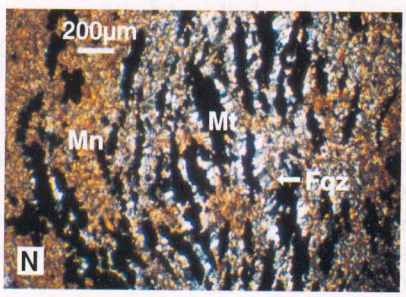
200µm
Mn
Mt
Fqz
N

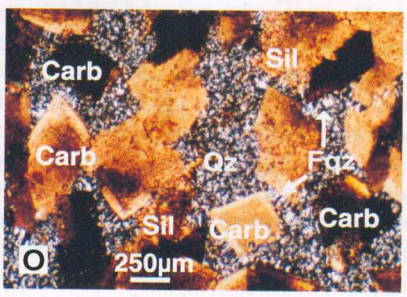
Carb
Sil
Carb
Qz
Fqz
Sil
Carb
Carb
250µm
O

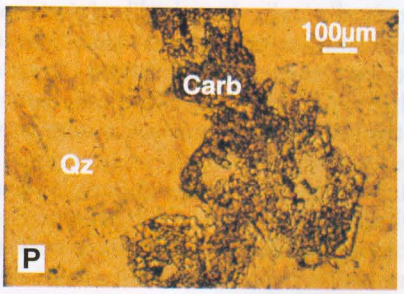
100µm
Carb
Qz
P

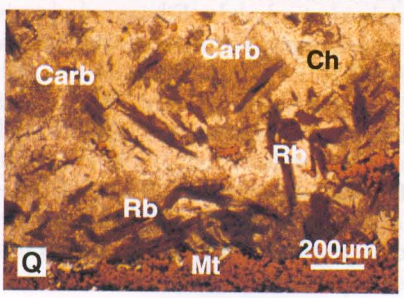
Carb
Carb
Ch
Rb
Rb
Mt
200µm
Q

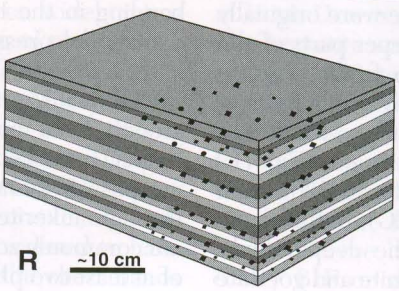
~10 cm
R

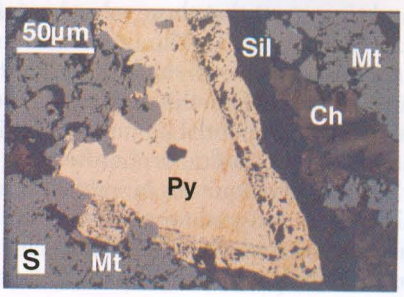
50µm
Sil
Mt
Ch
Py
Mt
S

The orebodies are overlain locally by low-grade West Angelas ore with very rare inclusions of cherty BIF and are bounded by very strongly weathered cherty BIF. No unoxidized or unweathered ore has been found at Hope Downs. The contacts are typically sharp and marked by the cut-off of well-defined chert bands. Most of the minor orebodies occur within the upper part of the Mount Newman Member and rarely occur below the NS3 silicate-chert-carbonate band (Figs. 3, 6).

The buried valley to the north of the ore deposit (Fig. 2) contains a variety of colluvial and alluvial detrital materials, including the Robe Pisolite Formation, Fe-rich scree, rounded hematite clasts in red ochreous hematite and clay matrix (ROD or red ochre detritals), bedded goethite and siderite, much of which is either ore grade or can be readily upgraded. Siderite deposits with ~35 wt percent Fe are self enriching to >60 wt percent Fe when exposed to the atmosphere. The underlying Wittenoom Dolomite is commonly replaced by ooidal siderite to depths in excess of 10 m but typically has high manganese content (2–20 wt %). High-grade scree deposits commonly occur around the lower slopes and adjacent to ore outcrops but the most recent surficial scree and alluvial sediments contain abundant chert clasts. Thick deposits (>100 m) of Fe-rich scree and red ochre detritals were also found in the valley on the south side of the Weeli Wolli anticline. The low-grade and detrital ores are not included in the reserves but are a probable future resource that together with high-grade ore in the Brockman Formation could conceivably double the life of the mine.

Ore petrography

The description of the ore is based on numerous field exposures, underground openings (adit and winzes), and diamond core. Polished thin sections were made of samples from the deeper parts of the ore deposits in order to avoid the more extreme weathering associated with soil-forming processes.

Martite is abundant throughout the ore, ranging from massive mesobands of interlocking grains to thin microbands and isolated euhedral grains. The martite trellis texture is very hard to distinguish in unweathered martite grains, as the martite is typically only very weakly anisotropic. However, the larger hematite crystallites are more resistant to hydration than the finer grained to amorphous interstitial hematite, and partial hydration clearly reveals the trellis texture (Fig. 7C) as well as the internal structure of the magnetite grains, many of which are shown to be euhedral overgrowths on primary microlaminae (Fig. 7D). The primary laminae are commonly highly brecciated with several fragments within the same magnetite aggregate (Fig. 7E). Rare traces of martite trellis structures occur within these microlaminae and no evidence was found to suggest that these microlaminae were originally hematite (cf. Han, 1978). The ore in the deeper parts of the deposit consists mainly of highly porous to friable martite with minor interstitial goethite. Approximately 15 vol percent consists of minor interstitial limonite and thin limonite bands. Limonite-goethite pseudomorphs after iron silicates (Fig. 7F) and carbonate are ubiquitous in weathered cherty BIF and in the shallow medium-grade orebodies (Fig. 7G), but limonite is mainly confined to thin mesobands in the deeper high-grade ore with only minor disseminated limonite and goethite in the hematite. The limonite that is pseudomorphous after iron silicate is rapidly converted to goethite through dehydration and crystallization, but the less coherent amorphous limonite derived from carbonate appears to persist longer in the saprolite, requiring dispersion and reprecipitation before crystallization occurred. No kenomagnetite (Morris, 1980) was observed in any of the ore samples.

Goethite shows a wide range of textures, including pseudomorphs of silicates, (Fig. 7F) carbonates (Fig. 7G), pyrite and martite (Fig. 7H), minor amorphous goethite bands (Fig. 7J) probably after fine-grained carbonate bands (cf. Fig. 5N, P c), and cementation (tertiary goethite) in deep saprolite ore, variably leached secondary goethite derived from the in situ dehydration of limonite (Fig. 7F) and tertiary (transported) infill goethite at shallower depths, and resinous nodules derived from the silicate-chert-carbonate bands. Above the water table, abundant crystalline to colloform goethite (Fig. 7F, K) fills voids between martite grains and replaces goethite and limonite after silicates and carbonates. Dissolution, dispersion, and redeposition of both secondary goethitic pseudomorphs and tertiary fillings also have occurred above the water table, characterized by several generations of tertiary botryoidal to microcrystalline goethite and increasing disruption of the primary textures. Traces of anhedral and cryptocrystalline (ochreous) hematite occur near the surface (Fig. 7K).

Cherty BIF petrography

Cherty BIF was sampled in completely unweathered BIF from diamond drill core outside the orebodies. Magnetite is abundant as subhedral to euhedral grains up to 200 μm in diameter, typically aggregated into laminae that form mesobands (Fig. 5A) but also as sheets as thin as 10 μm and as disseminations. Inclusions of hematite are not seen in completely unweathered magnetite (Fig. 5A, B) but commonly appear at the earliest stages of weathering together with fringing hematite (Fig. 7L). Massive mesobands are typically distorted and brecciated with pressure shadows of fibrous quartz developed between the fragments (Fig. 7M). Apart from the pressure shadows interstitial quartz is typically absent from magnetite mesobands (Fig. 6A, B).

Magnetite-silicate BIF is abundant in the MacLeod and Nammuldi Members with micron-scale quartz crystals ranging from minor disseminations or patches in silicate bands to complete mesobands. Finely laminated magnetite-silicate mesobands are typically crumpled or broken, with delamination (Hippertt et al., 2001) and abundant fibrous quartz (cross-fiber) lenses between laminae (Fig. 7N), whereas the silicate laminae show little or no disruption, although oriented acicular crystals occur locally at high angles to the banding in the thicker mesobands. Fibrous quartz is abundant in the pressure shadows of isolated grains of magnetite and carbonates (Fig. 7O).

Carbonate grains within chert bands show all stages of growth from euhedral rhomboids (Fig. 7O) to anhedral, largely replaced skeletal relics (Fig. 7P) to quartz pseudomorphs (Fig. 5M) and range in composition from siderite through ankerite and dolomite to calcite. Individual crystals are commonly zoned (Fig 7O) and typically display exsolution of at least two phases, producing a granular internal structure

of siderite and dolomite (Fig. 7P) commonly fringed by ankerite or calcite. All four species of carbonate may be present in the same thin section. Ghost laminations of fine carbon or stilpnomelane in coarsely crystalline carbonate bands, veins, and breccias indicate in situ replacement of silicate mesobands by carbonate (Fig. 5G, H) that may subsequently be replaced by microquartz (Fig. 5M). Chert bands typically show greater abundance of carbonate grains toward the outside of the band but contacts with other mesobands are typically sharp with mixed carbonate-silicate bands commonly occurring between chert and magnetite mesobands. Interstitial silica in the mixed bands is rare and almost cryptocrystalline, except where microcrystalline (~30 μm, Fig. 5M) quartz is pseudomorphous after carbonate grains.

Minnesotaite (Figs. 5B, M, 7M, N) is the predominant iron silicate mineral in the BIF macrobands. It occurs interstitial to magnetite, as discrete mesobands largely replaced by chert, partially replaced by carbonate in the carbonate-silicate bands and as traces in chert mesobands. Stilpnomelane is widely distributed as a trace interstitial mineral and in rare laminae throughout the BIF macrobands. However, riebeckite is abundant in the Mount Newman Member at Hope Downs and is commonly the sole iron silicate mineral in the most intensely deformed areas. It occurs as fine fibers distributed in oriented bands within chert, as long fibers between lenticular augen in mylonitic zones, and as prismatic crystals with frayed fibrous terminations (Fig. 7Q) along contacts between magnetite and chert mesobands, as well as the asbestiform seams.

Pyrite is locally abundant, occurring as large (<2 mm) crystals and as disseminated minute (<10 μm) crystals (Fig. 7L). It is typically anhedral against magnetite and euhedral against silicates, carbonates, and chert. Euhedral magnetite rarely shows well-formed octahedra or cubes with intersecting and twinned dodecahedra being the most common habit, whereas well-formed cubic and octahedral pyrite is typical (Fig. 7L) and goethite pseudomorphous after pyrite can commonly be distinguished by the outline as well as the internal structure (Blanchard, 1968). Although very rarely in vein form, and with the grains typically grouped along the undersurface of magnetite mesobands or disseminated in silicate and chert bands, pyrite nevertheless shows a strong vertical distribution perpendicular to the bedding (Fig. 7R). Rare anhedral to colloform overgrowths on some euhedral pyrite grains suggest two stages of sulfide input (Fig. 7S). Pyrite clearly shows greater resistance to oxidation than iron silicates or magnetite (Fig. 7L). Rare anhedral grains of chalcopyrite are present as a trace constituent associated with the pyrite.

Discussion

High-grade hematite ore deposits have been widely interpreted to be products of supergene leaching of chert bands from BIF (Van Hise and Leith, 1911; MacLeod, 1966; Morris, 1980, 1985, 2002; Harmsworth et al., 1990; Morey, 1999). Hydrothermal processes also have been shown to be important in the formation of some of the larger deposits (Dalstra and Guedes, 2004), in particular those containing micaceous specular hematite and some microplaty hematite ores, although martite-goethite deposits are still considered to have formed by selective supergene leaching of the chert bands (Taylor et al., 2001; Klein and Ladeira, 2002, 2004; Clout, 2005; Hannan et al., 2005). The supergene model is commonly compared to the origin of bauxitic and lateritic soils on siliceous rocks, although they lack any preservation of primary textures, and quartz, if present, is completely unaltered in the underlying saprolite. Ollier and Galloway (1990) have questioned both the residual nature of bauxite and laterite and the large-scale dissolution of quartz by lateritic weathering based on unconformable relationships of the soils to the underlying saprolite.

Major iron ore deposits extend to great depths within the saprolite with full preservation of primary textures. High-grade ore extending to more than 200 m below the water table at Hope Downs shows no sign of soil-forming processes and the water table appears to be at its lowest ever level.

Origin of the high-grade ore deposits at Hope Downs

All the high-grade ore lies within the deeply weathered regolith and consists of saprolite in which fine textures are well preserved. Textures of the martite-goethite and limonitic mesobands derived from the weathering of carbonate-silicate mesobands in both ore and cherty BIF are identical across the contacts. Only in the upper levels (B soil horizon) where mobilization of goethite, hematite, and hydration of martite has occurred is the ore cemented by secondary goethite or hematite to produce massive or poddy conchoidal-fracturing martite-hematite-goethite ore.

Weathered cherty BIF with complete chert bands is in sharp contact with the ore, and any feathering or decrease in the chert content occurs over a span of a few microns to millimeters. The white, typically friable chert bands in the saprolite (Fig. 8A) show no evidence of replacement by goethite, although such replacement is abundant in upper soil horizons whereas extreme leaching in BIF saprolite results in removal of all iron oxides to leave bleached chert sequences. Ferruginous hardcaps on cherty BIF commonly simulate weathered high-grade ore but evidence of the former presence of chert bands in the form of voids and minor chert remnants is typically present. No such evidence of chert bands is ever seen in high-grade ore (Fig. 8B).

Certain ore deposits clearly show hydrothermal replacement of resistant chert bands by easily weathered carbonate (Griffin, 1980; Lascelles, 2002; Dalstra and Guedes, 2004) but no evidence could be found of complete carbonate replacement of chert bands at Hope Downs, where interaction of carbonate with minnesotaite (Fig. 5G, H) and quartz (Fig. 5M) occurred on a relatively minor scale. Hot brines may have been involved in the sodium metasomatism that formed the riebeckite, but they appear to have been of local derivation and no other evidence of hydrothermal action was seen at Hope Downs. In particular, no trace of microplaty or specular hematite was observed.

Drill hole intersections of chert-free carbonate facies BIF (up to 2 m) consisting of carbonates interlayered with iron silicate and minor fine-grained magnetite capable of weathering to low-grade ore were observed in both the MacLeod and Nammuldi Members. Although no unweathered high-grade ore (chert-free BIF) has been intersected at Hope Downs where the ore is invariably underlain by deeply weathered cherty BIF or shale, the ore is essentially similar to other

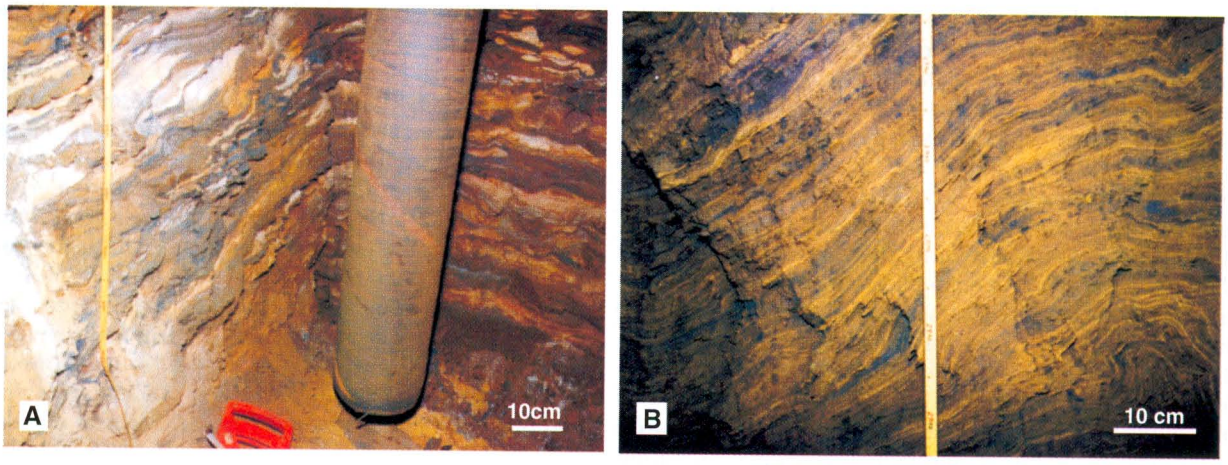

FIG. 8. Exposures of the Mount Newman Member from winzes at Hope Downs north deposit (plateau area). A. Cherty BIF saprolite (depth 44 m). B. High-grade ore (depth 29 m) from Lascelles (2002; photos courtesy of Hancock Resources Ltd.).

deposits in the Hamersley province that are underlain by partially weathered chert-free magnetite BIF. A clear contact between unweathered cherty and chert-free BIF is illustrated in figure 11A of Taylor et al. (2001). Inspection of this core sample by the author suggested that the carbonates interlaminated with the magnetite are remnants of carbonate-rich chert bands and that no chert bands were replaced by carbonate. The numerous crosscutting carbonate veins in the chert-free portion are apparently fracture fills in the autobrecciated chert-free BIF, possibly due to the blocking of dewatering channels by carbonate grains.

Sedimentation of BIF

In a previous study of Mount Gibson (Lascelles, 2006), it was shown that the differentiation between chert-free and cherty BIF took place prior to metamorphism and regional deformation. It was suggested that the initial precipitate consisted mainly of iron hydroxide and Al-poor nontronite and was deposited around hydrothermal vents on the sea floor and that the chert bands formed by dissociation of the nontronite into iron oxide and gelatinous silica during diagenesis. However, modern deposits in the vicinity of many undersea hydrothermal vents bear no comparison to BIF as they consist of unlaminated and unsorted mounds of precipitated Fe and Mn hydroxyoxides and silicates (Fig. 9A) around sulfidic chimneys (Parr et al., 2003). Mineralogical sorting into laminae and bands occurs during resedimentation (Paolo et al., 1989) by turbidity (Fig. 9B, C) and density currents (Fig. 9D)

Abundant evidence of current transport and deposition at Hope Downs (Fig. 5N, P) indicates that the components of BIF have been reworked from their original site of precipitation (cf. Hyde, 1980; Meyn and Palonen, 1980; Barrett and Fralick, 1985, 1989; Krapez et al., 2003; Pickard et al., 2004) and a number of features confirm deposition by episodic rather than continuous currents. The silicification of shale horizons and upper surfaces of BIF macrobands is interpreted as sediment-seawater interaction during periods of slow or nondeposition (hardgrounds: Krapez et al., 2003) and the presence of scours and ripups (Fig. 5P) are indicative of rapid change from still conditions to fast-moving currents.

Hydrous iron aluminosilicate (smectite) flocculates and crystallizes more rapidly after formation than hydrous Al-poor iron silicate (nontronite) and iron hydroxides (Caldwell and Marshall, 1942) and consequently has larger grain size, faster settling rates, and typically forms the base of each density-current sequence. BIF sequences at Hope Downs typically commence with shales and mud rocks at the base and commonly show minor erosion of the underlying sediment with shallow scouring, rip-outs (Fig. 5P) and truncated ripple marks in underlying finely laminated BIF. They commonly contain abundant globular chert pods interpreted to be derived from clasts of gelatinous silica accumulated on the sea floor that were swept up by the current together with subrectangular clasts derived from the silicified water-sediment interface (Fig. 5P). The source of the gelatinous silica is uncertain, whether from direct precipitation from seawater (e.g., Moore and Maynard, 1929; Grenne and Slack, 2005) or by the escape of amorphous silica from chert bands during the formation of chert-free BIF; however, the presence of similar chert pods in the underlying Jeerinah Formation suggests the former is common. Laminations in the shale are typically continuous around these chert clasts and evidence of hardened skins and internal shrinkage cracks indicate their contemporaneous deposition in contrast to pods derived from replacement of silicate, syneresis or deformation of chert bands, or siliceous concretions, which typically show conformable internal laminations. Fine-grained carbonate and iron silicate layers containing minor interstitial iron aluminosilicate, followed by the still finer grained colloidal iron hydroxide and minnesotaite BIF, typically follow the basal stilpnomelane-rich shale or mud rocks.

More detailed descriptions of the Marra Mamba Iron Formation presented in Lascelles (2000) shed light on the deposition at Hope Downs. The cherty BIF in the lower Mount Newman Member appears to have been deposited during a more stable period when lithification of the iron oxides and silica gel progressed to the point of well-defined laminae that behaved in a less fluid manner during creep. Chert-free BIF is much less widespread than in the upper part of the Member, and numerous lenses of fibrous quartz

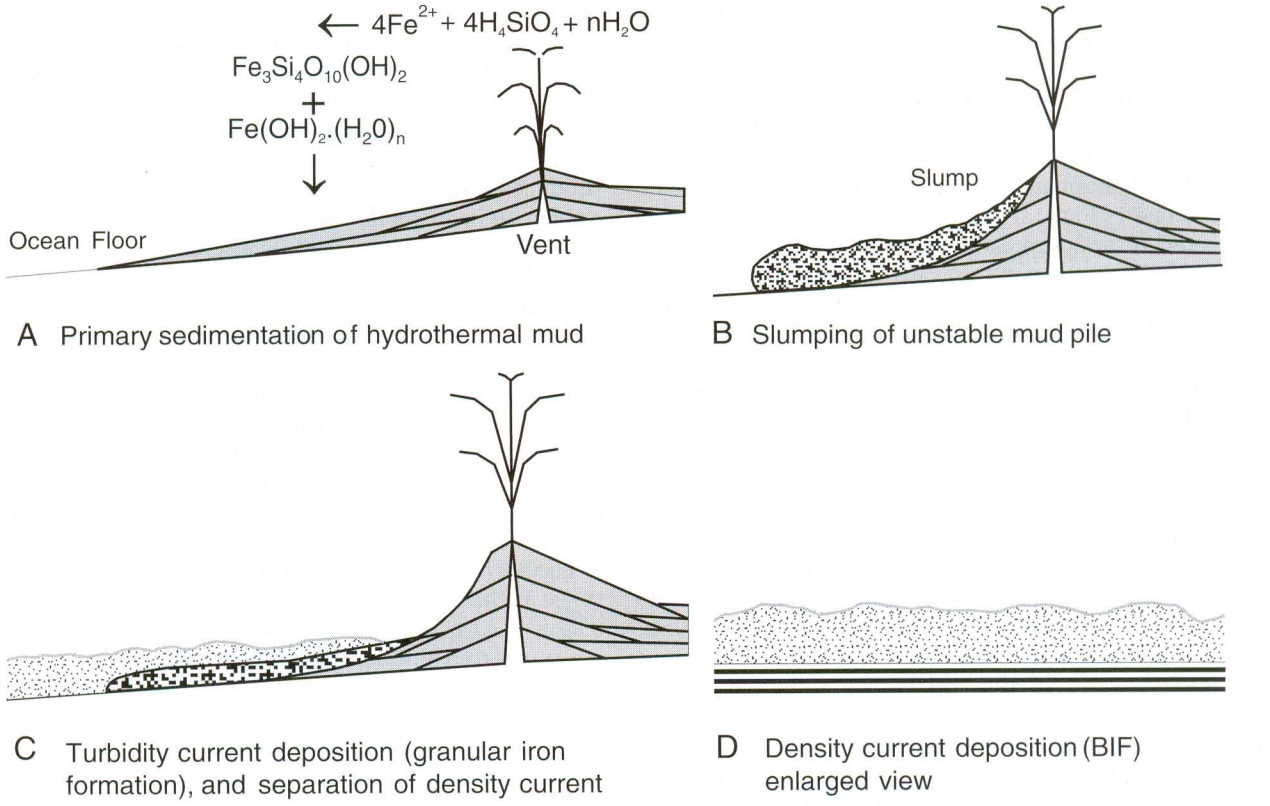

FIG. 9. Schematic diagram showing sedimentation of iron-formation.

point to the abundance of silica-saturated pore water derived from syneresis of the chert bands. However, the overall texture of the banding is similar to the MacLeod and Nammuldi Members, with their clear evidence of current deposition, and the stratigraphy and textures of BIF are compatible with those of fine-grained turbidites (Stow and Bowen, 1980; Paolo et al., 1989; Bouma, 2000). The characteristic microlamination of iron oxides and iron silicates is produced by semiregular fluctuations in current velocity (Paolo et al., 1989).

Banding and fine lamination is less obvious in the silicate-chert-carbonate bands but is well developed in dolomitic shales (Fig. 10) and carbonates in the overlying West Angela Member, which display typical fine-grained turbidity-current sedimentation (Bouma, 2000), marking a change from colloidal density current deposition to fine-grained particulate sedimentation. The thick carbonate-rich silicate-chert-carbonate bands in the Marra Mamba Iron Formation are assumed to have a similar origin of more distal density-current deposition derived from a carbonate-mud source area. Black shale and medium-grained carbonate bands are more common in the MacLeod and Nammuldi Member silicate-chert-carbonate units.

The tuffaceous and coarse-grained horizons in the Brockman Formation S bands (Pickard et al., 2001, 2004) are not known from the Marra Mamba Iron Formation, which suggests that the Formation was deposited under calmer conditions distal to the source of the density currents, and the coarse mesobanding suggests deposition from slow-moving density currents as the colloidal suspensions flocculated and settled out. This may also explain the lower phosphorous content of the Marra Mamba Iron Formation, as apatite grains from the source were deposited proximally and only neoformed apatite or colloidal particles were codeposited with the Marra Mamba Iron Formation. Numerous creep and soft-sediment slump structures suggest that the Formation was deposited on a gently sloping surface and appear to have occurred by stretching of the sediments as no breaks in the stratigraphic sequence have been observed and the planar chert bands are typically thinly bedded compared to the more contorted chert bands. The iron oxide layers typically show a higher degree of plasticity during slumping, with the iron oxide anastomozing around chert pods (Fig. 5F, Q), but there

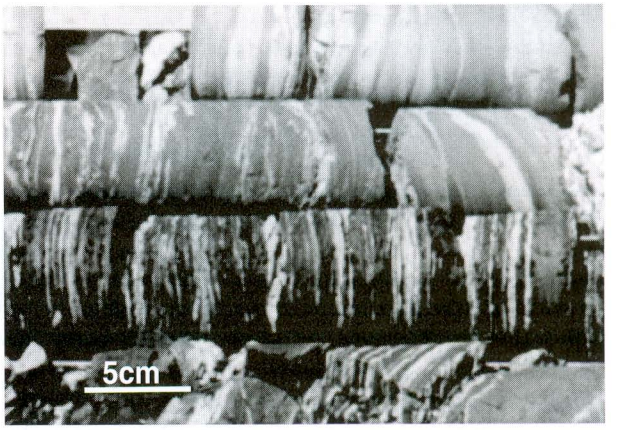

FIG. 10. Banded dolomitic shale from the West Angela Member (AS3).

is abundant evidence of plasticity in the chert with simultaneous distortion and boudinaging. Slumping and creep are less apparent in ore where collapse structures, brecciation, and small-scale folding are more common.

In models discussed in Lascelles (2002, 2006), the breakdown of nontronite during diagenesis of the transported sediment produced abundant gelatinous silica that accumulated as bands of chert (Fig. 11A-C). The hydrophobic iron oxide laminae acted as semipermeable membranes (Marshall, 1949; Hiemenz, 1997), preventing upward movement of the hydrophilic gelatinous silica. The fine particles of stilpnomelane, iron oxides, and carbon (Fig. 5C) that form traces of bedding within the chert resulted from stable impurities remaining after the diagenetic dissociation of the nontronite. The high density of the iron oxide laminae overlying gelatinous silica layers produced an unstable pile of sediments. Pinch and swell structures in the gelatinous layers (Fig. 5D,) were then exaggerated by compaction pressures and syneresis while gravity induced creep and slumping produced further distortion (Fig. 5F, Q). Breaches of the iron oxide laminae allowing the escape of gelatinous silica provided a simple mechanism for the formation of residual chert-free BIF (Fig. 11D). Subsequent collapse of the overlying sediment induced further fracturing up to the top of the sediment (i.e., a domino effect), producing large volumes of chert-free BIF.

The initial precipitate of hydrous iron hydroxide crystallized as anhedral fine-grained aggregates that developed euhedral overgrowths of magnetite during diagenesis and metamorphism. During oxidation the fine-grained material was rapidly oxidized giving rise to inclusions of hematite in magnetite (Fig. 7L) that are absent in completely unweathered BIF (Fig. 5A) but have previously been identified as primary hematite (Han, 1978; Morris, 1985).

Most of the silicate minerals in the BIF at Hope Downs appear to be the products of diagenesis and metamorphism of the original sediment (nontronite → greenalite → minnesotaite; chamosite → stilpnomelane) and, unlike Mount Gibson, no evidence was found of postdeposition reactions between quartz and magnetite, except perhaps for the growth of crocidolite. Metasomatism by saline connate water heated by intrusive sills or underlying basalt flows is thought to have produced local concentrations of hot (>150°C) brines that reacted with iron silicate bands to form riebeckite (Grubb, 1971). Overpressured brines containing dispersions of silica produced local inflation of iron oxide mesobands and, rarely, riebeckite bands, followed by the growth of crocidolite fibers by reaction with the iron oxide laminae. The brittle fracturing of oxide laminae by fiber growth (Fig. 7J) indicates that the asbestiform seams developed after lithification but prior to the regional folding. The predominance of riebeckite as the iron silicate mineral in the mylonitized zones suggests that sodium metasomatism also accompanied the formation of the thrusts. Abundant carbonate alteration present in the BIF is assumed to be due to diagenetic interaction of CO_2-rich connate water from the carbonate bands replacing the silicates and chert and reacting with iron oxides to form the interstitial siderite in the oxide mesobands.

The vertical distribution of pyrite within the BIF (Fig. 7R) suggests that it formed from migrating pore fluids containing dissolved H_2S. The preferential occurrence of pyrite on the lower surfaces of iron oxide mesobands indicates that this was an upward movement, and the absence of pyrite veins suggests that it occurred during the soft-sediment stage before the sediments could support fracturing.

Structural considerations in the origin of the ore at Hope Downs

Although the major orebodies at Hope Downs are associated with folding and thrusting in synclinal structures, continuations of the ore and numerous smaller deposits are in flat-lying relatively undisturbed structural areas. Similarly the cherty BIF occurs in both areas and shows equal or greater deformation than the ore.

The pattern of folding at Hope Downs of flattened anticlines and steeply dipping synclines (Fig. 2) is not unusual in the Hamersley province, particularly in the vicinity of ore

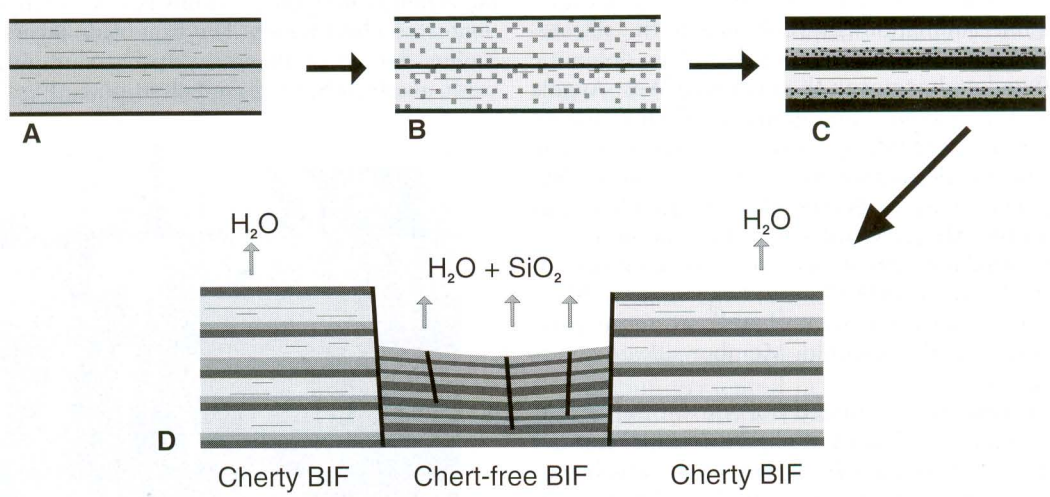

FIG. 11. Schematic diagram of BIF diagenesis, showing the possible origin of chert-free BIF. A. Deposition of nontronite and iron hydroxide. B. Breakdown of nontronite to iron oxide and colloidal silica. C. Settling of iron oxide and remnant iron silicate particles and entrapment of silica beneath iron hydroxide laminae forming mineralogical banding. D. Dewatering of sediment and escape of thixotropic colloidal silica up fractures in iron hydroxide laminae to form chert-free BIF.

deposits. If the origin of the chert-free BIF predates the regional folding then it is clear that the BIF was highly anisotropic in the region of the major ore deposits and that this would have affected the pattern of folding during the buckling of the strata. The association of the larger and higher grade ore deposits at Hope Downs with the southern limbs of synclines suggests that the more dense and less rigid chert-free BIF may have influenced the location of downwarps with the less dense cherty BIF tending to produce flat-lying to anticlinal forms. The lower grade ore, with abundant limonite derived from carbonate and silicate, has a lower density contrast with the cherty BIF and commonly occurs in the flat-lying to anticlinal areas. The low-angle thrusts appear to be late structures associated with the final stage of folding (D_{3cap} of Müller et al., 2005) and generally carry flat-lying cherty BIF and ore over the synclinal chert-free ore. Thus the ore may have controlled the structure instead of the structure controlling the location of the ore, but this would not apply to hydrothermal ore deposits that were contemporaneous or later than the folding and metamorphism (Dalstra, 2005).

Conclusions

The Marra Mamba Iron Formation at Hope Downs is interpreted to consist of a sequence of density-current deposits derived from a source of ultrafine colloidal iron oxides, iron silicates, and minor iron carbonates interspersed with turbidity density flows of fine-grained carbonates. Quiet intervals between density currents allowed minor accumulation of carbonaceous and pyritic pelagic shale with iron aluminosilicates and possibly precipitated carbonate ooze, with silicification of the sediment surface during periods of nondeposition. Erosion of the sea floor by successive density currents caused minor scouring, rip-outs, and truncated ripples. Small traces of stilpnomelane are ubiquitous throughout the formation and probably represent contamination by pelagic colloidal aluminosilicates during the precipitation of the iron oxides and silicates.

In this model the chert bands form during diagenesis of the sediments from the decomposition of Al-poor, Fe-rich smectites, releasing large quantities of amorphous silica that were trapped into horizontal layers by iron hydroxide laminae acting as semipermeable membranes. Fracturing of the membranes allowed the release of the colloidal silica and subsequent collapse of overlying sediment to produce various volumes of chert-free BIF.

Mobilization of iron in the deeper saprolite is restricted to dispersion of limonite and redeposition as goethite in the upper levels. The higher grades in the deeper parts are due to loss of low-grade hydroxides and not replacement of gangue by imported iron. No trace of the previous existence of chert bands can be found in saprolite ore; podding or voids where chert bands might have been were not observed, although all these features can be observed near the surface in weathered cherty BIF. Where present, chert bands are always complete, even if degraded to fine silt. These observations are incompatible with the currently accepted models of supergene enrichment by the selective leaching and replacement of chert bands by goethite. The observations at Hope Downs and Mount Gibson (Lascelles, 2006) suggest that the protore contained no chert. Supergene enrichment of in situ ore is restricted to the oxidation and leaching of carbonate and silicate minerals; in this model only chert-free BIF could form high-grade hematite ore through supergene processes. Both the high-grade martite-limonite ore from the Mount Newman and Nammuldi Members and the low-grade goethite-limonite ore from the West Angelas, MacLeod, and Nammuldi Members were formed by the weathering of chert-free BIF.

Acknowledgments

This research was conducted as part of a Ph.D. thesis on the origin of BIF and in situ-derived iron ore deposits at the Centre for Exploration Targeting, University of Western Australia. The fieldwork was carried out while employed as a consultant geologist by Hancock Resources Pty. Ltd., who provided access to diamond core, company reports and records, and in concert with joint venture partners Rio Tinto Iron Ore, who kindly gave permission to publish this paper. The constructive criticism by M.E. Barley and reviewers, especially H. Dalstra, is gratefully acknowledged. F. Talen drafted the original versions of Figures 1 and 3.

May 7, 2004; October 2, 2006

REFERENCES

Barrett, T.J., and Fralick, P.W., 1985, Sediment redeposition in Archaean iron-formation: Examples from the Beardmore-Geraldton greenstone belt, Ontario: Journal of Sedimentary Petrology, v. 55, p. 205–212.

——1989, Turbidites and iron formations, Beardmore-Geraldton, Ontario: Application of a combined ramp/fan model to Archaean clastic and chemical sedimentation: Sedimentology, v. 36, p. 221–234.

Beukes, N.J., 1980, Lithofacies and stratigraphy of the Kuruman and Griquatown iron-formations, northern Cape Province, South Africa: Transactions of the Geological Society of South Africa, v. 83, p. 69–86.

Blanchard, P., 1968, The interpretation of leached outcrops: Nevada Bureau of Mines, Bulletin 66, 196 p.

Blockley, J.G., Tehnas, I.J., Mandyczewsky, A., and Morris, R.C., 1993, Proposed stratigraphic subdivisions of the MMIF and the lower Wittenoom Dolomite, Hamersley Group, Western Australia: Western Australian Geological Survey Report 34. p. 47–63.

Bouma, A. H., 2000, Fine-grained mud-rich turbidite systems: Model and comparison with coarse-grained sand-rich systems: American Association of Petroleum Geologists Memoir 72, p. 9–19.

Caldwell, O.G., and Marshall, C.E., 1942, A study of some chemical and physical properties of the clay minerals nontronite, attapulgite and saponite: Missouri University College Agricultural Research Bulletin 354.

Clout, J.M.F., 2005, Iron formation hosted iron ores in the Hamersley province of Western Australia: Australasian Institute of Mining and Mineralogy Publication 8/2005, p. 9–19.

Compston, W., Williams, I.S., McCulloch, M.T., Foster, J.J., Arriens, P.A., and Trendall, A.F., 1981, A revised age for the Hamersley Group [abs.]: Geological Society of Australia, 5th Annual Convention, Perth, Abstracts, v. 3, p. 40.

Dalstra, H.J., 2005, Structural controls of bedded iron ore in the Hamersley province, Western Australia—an example from the Paraburdoo Ranges: Australasian Institute of Mining and Mineralogy Publication 8/2005, p. 49–55.

Dalstra, H., and Guedes, S., 2004, Giant hydrothermal hematite deposits with Mg-Fe metasomatism: A comparison of the Carajas, Hamersley, and other iron ores: Economic Geology, v. 99, p. 1793–1800.

Davy, R., 1975, A geochemical study of a dolomite-BIF transition in the lower part of the Hamersley Group: Western Australian Geological Survey Annual Report for 1974, p. 128–140.

Davy, R., and Hickman, A.H., 1988, The transition between the Hamersley and Fortescue Groups as evidenced in a drill core: Western Australian Geological Survey Professional Papers, p. 85–97.

Grenne, T., and Slack, J.F., 2005, Geochemistry of jasper beds from the Ordovician Løkken Ophiolite, Norway: Origin of proximal and distal siliceous exhalites, Economic Geology, v. 100, p. 1511–1527.

Griffin, A.C., 1980, Structural geology and sites of iron ore deposition in Koolyanobbing Range, Western Australia: International Archaean Symposium, 2nd, Archaean Geochemistry Project, Perth, Proceedings, p. 64–65.

Grubb, P.L.C., 1971, Silicates and their paragenesis in the Brockman Iron Formation of Wittenoom Gorge, Western Australia: Economic Geology, v. 66, p. 281–294.

Han, T-M., 1978, Microstructures of magnetite as guides to its origin in some Precambrian iron-formations: Fortschritte der Mineralogie, v. 56, p. 105–142.

Hannon, E., Kepert, D.A., and Clark, D., 2005, From target generation to two billion tonnes in 18 months—the re-invention of the Chichester Range: Australasian Institute of Mining and Metallurgy Publication Series 8/2005, p. 73–77.

Harmsworth, R.A., Kneeshaw, M., Morris, R.C., Robinson, C.J., and Shrivastava, P.K., 1990, BIF-derived ores of the Hamersley province: Australasian Institute of Mining and Metallurgy Monograph 14, v. 1, p. 617–642.

Hiemenz, P.C., 1997, Principles of colloid and surface chemistry, 3rd ed.: New York, Marcel Dekker, 650 p.

Hippertt, J., Lana, C., and Takeshita, T., 2001, Deformation partitioning during folding of banded iron formation: Journal of Structural Geology, v. 23, p. 819–834.

Hyde, R.S., 1980, Sedimentary facies in the Archean Timiskaming Group and their tectonic implications, Abititbi greenstone nelt, northeastern Ontario, Canada: Precambrian Research, v. 12, p. 161–195.

Jackson, J.A., 1997, Glossary of geology, 4th ed.: Alexandria, Virginia, American Geological Institute, 769 p.

James, H. L., 1954, Sedimentary facies of iron formation: Economic Geology, v. 49, p. 235–293.

Klein, C., and Ladeira, E.A., 2002, Petrography and geochemistry of the least altered banded iron-formation of the Archean Carajás Formation, northern Brazil: Economic Geology, v. 97, p. 643–651.

——2004, Geochemistry and mineralogy of Neoproterozoic banded iron-formations and some selected siliceous manganese formations from the Urucum district, Matto Grosso do Sul, Brazil: Economic Geology, v. 99, p. 1233–1244.

Krapez, B., Barley, M.E., and Pickard, A.L., 2003, Hydrothermal and resedimented origins of the precursor sediments to banded iron formation: Sedimentological evidence from the Early Palaeoproterozoic Brockman Supersequence of Western Australia: Sedimentology, v. 50, p. 979–1011.

La Berge, G.L., 1966, Altered pyroclastic rocks in iron formation in the Hamersley Range, Western Australia: Economic Geology, v. 61, p. 147–161.

Lascelles, D.F., 2000, Marra Mamba Iron Formation stratigraphy in the eastern Chichester Range, Western Australia: sof Earth Science, v. 47, p. 799–806.

——2002, A new look at old rocks: A non-supergene origin for BIF-derived in situ high-grade iron ore deposits: Australasian Institute of Mining and Mineralogy Publication 8/2005, p. 107–126.

——2006, The Mount Gibson banded iron-formation hosted magnetite deposit: Two distinct processes for the origin of enriched iron ore deposits: Economic Geology, v. 101, p. 651–666.

MacLeod, W.N., 1966, The Geology and iron deposits of the Hamersley Range area, Western Australia: Geological Survey of Western Australia Bulletin 117119, 170 p.

Marshall, C.E., 1949, The colloid chemistry of the silicate minerals: Agronomy Monograph ix, vo. 1: New York, Academic Press, 195 p.

Meyn, H.D., and Palonen, P.A., 1980, Stratigraphy of an Archaean submarine fan: Precambrian Research, v. 12, p. 257–285.

Miyano, T., 1987, Diagenetic to low-grade metamorphic conditions of Precambrian iron-formations, *in* Appel, P.W.U., and La Berge, G.L., eds., Precambrian iron-formations: Athens, Theophrastus Publications, S.A., p. 155–186.

Moore, E.S., and Maynard, J.E., 1929, Solution, transportation and precipitation of iron and silica: Economic Geology, v. 24, p. 272–303, 365–402, 506–527.

Morey, G.B., 1999, High-grade iron ore deposits of the Mesabi Range, Minnesota—product of a continental-scale Proterozoic ground-water flow system: Economic Geology, v. 94, p. 133–142.

Morris, R.C., 1980, A textural and mineralogical study of the relationship of iron ore to banded iron-formation in the Hamersley iron province of Western Australia: Economic Geology, v. 75, p. 184–209.

——1985, Genesis of iron ore in banded iron-formation by supergene and supergene-metamorphic processes—a conceptual model, *in* Wolf, K.H., ed., Handbook of strata-bound and stratiform ore deposits, 13: Amsterdam, Elsevier, p. 73–235.

——1991, The Marra Mamba Iron Formation of the Hamersley Group of Western Australia: Perth, Commonwealth Scientific and Industrial Research Organization, Exploration Geoscience Restricted Report 158R, 230 p.

——2002, Iron ore genesis and post-ore metasomatism at Mount Tom Price: Australasian Institute for Mining and Metallurgy Publication 8/2005, p. 3–14 (reprinted in Transactions of the Institution of Mining and Metallurgy, v. 112, sec B: Applied Earth Science).

Müller, S.G., Krapez, B., Barley, M.E., and Fletcher, I.R., 2005, Giant iron-ore deposits of the Hamersley province related to the breakup of Paleoproterozoic Australia: New insights from in situ SHRIMP dating of baddeleyite from mafic intrusions: Geology, v. 33, p. 577–580.

Ollier, C.D., and Galloway, R.W., 1990, The laterite profile, ferricrete and unconformity: Catena, v. 17, p. 97–109.

Paolo, C., Wiele, S.M., and Reinhart, M.A., 1989, Upper regime parallel lamination as the result of turbulent sediment transport and low-amplitude bed forms: Sedimentology, v. 36, p. 47–59.

Paquay, R.D., and Ness, P.K., 1998, Hope Downs iron ore deposits: Australasian Institute of Mining and Metallurgy Monograph 22, p. 381–386.

Parr, J., Yeats, C., and Binns, R., 2003, Petrology, trace element geochemistry and isotope geochemistry of sulfides and oxides from the PACMANUS hydrothermal field, Eastern Manus basin, Papua New Guinea: North Ryde, Australia, CSIRO Exploration and Mining Report 1112F, p. 53–57.

Pickard, A.L., Krapez, B., and Barley, M.E., 2001, Dales Gorge Member S macrobands—what are they and why are they important? [ext. abs.]: International Archaean Symposium 2001, 4th, Perth, 2001, Extended Abstracts, p. 256–258.

Pickard, A.L., Barley, M.E., and Krapez, B., 2004, Deep-marine depositional setting of banded iron formation: Sedimentological evidence from interbedded clastic sedimentary rocks in the early Palaeoproterozoic Dales Gorge Member of Western Australia: Sedimentary Geology, v. 170, p. 37–62.

Richards, J.R., and Blockley, J.G., 1984, The base of the Fortescue Group, Western Australia: Further galena lead isotope evidence on its age: Australian Journal of Earth Sciences, v. 31, p. 257–268.

Smith, R.E., Perdrix, J.L., and Parks, T.C., 1982, Burial metamorphism in the Hamersley basin, Western Australia: Journal of Petrology, v. 23, p. 75–102.

Stow, D.A.V., and Bowen, A.J., 1980, A physical model for the transport and sorting of fine-grained sediment by turbidity-currents: Sedimentology, v. 27, p. 31–46.

Taylor, D., Dalstra, H.J., Harding, A.E., Broadbent, G.C., and Barley, M.E., 2001, Genesis of high-grade hematite orebodies of the Hamersley province, Western Australia: Economic Geology, v. 96, p. 837–873.

Trendall, A.F., 1979, A revision of the Mount Bruce Supergroup: Geological Survey of Western Australia, Annual Report for 1978, p. 63–71.

Trendall, A.F., and Blockley, J.G., 1970, The iron formations of the Precambrian Hamersley Group, Western Australia, with special reference to the associated crocidolite: Geological Survey of Western Australia Bulletin 119, p. 366 p.

Trendall, A.F., Compston, W., Nelson, D.R., de Laeter, J.R., and Bennett, V.C., 2004, SHRIMP zircon ages constraining the depositional chronology of the Hamersley Group, Western Australia: Australian Journal of Earth Sciences, v. 51, p. 621–644.

Tyler, I.M., and Thorne, A.M., 1990, The northern margin of the Capricorn orogeny, Western Australia—an example of an early Proterozoic collision zone: Journal of Structural Geology, v. 12, p. 685–701.

Van Hise, C.R., and Leith, C.K., 1911, The geology of the Lake Superior region: U.S. Geological Survey Monograph 52, p. 641 p.

Webb, A.D., Dickens, G.R., and Oliver, N.H.S., 2003, From banded iron-formation to iron ore: Geochemical and mineralogical constraints from across the Hamersley province, Western Australia: Chemical Geology, v. 197, p. 215–251.

Yariv, S., and Cross, H., 1979, Geochemistry of colloid systems: New York, Springer-Verlag, 450 p.